AD-A055 622 PHRASOR TECHNOLOGY PASADENA CA F/G 20/8
MECHANISMS OF EMITTER SURFACE DAMAGE DURING ELECTROHYDRODYNAMIC--ETC(U)
MAR 78 J F MAHONEY, J PEREL, B E KALENSHER F44620-75-C-0056
UNCLASSIFIED AFOSR-TR-78-1026 NL

| OF |
AD
A055 622

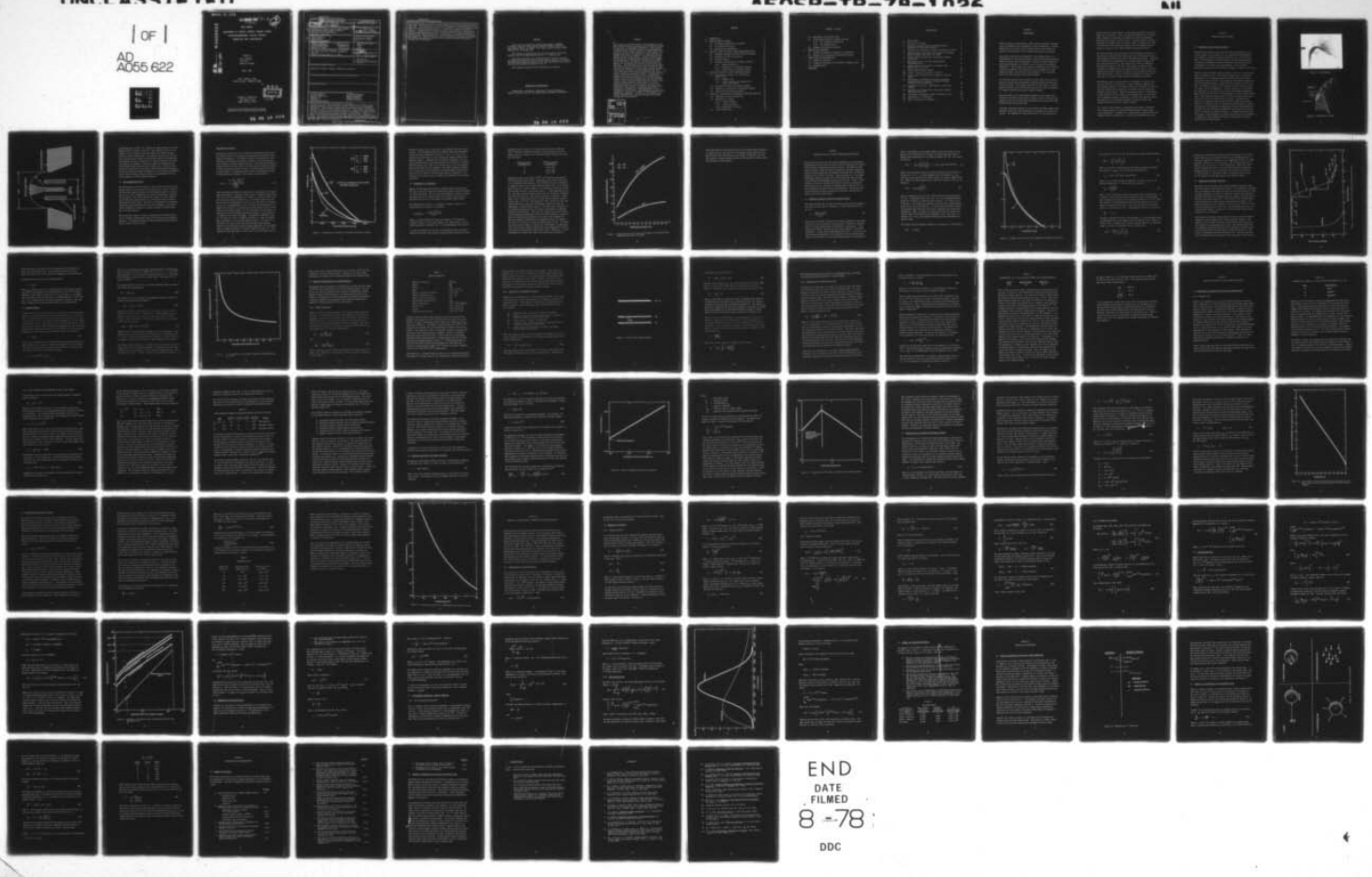

END
DATE FILMED
8-78
DDC

FINAL REPORT

MECHANISMS OF EMITTER SURFACE DAMAGE DURING ELECTROHYDRODYNAMIC COLLOID PARTICLE GENERATION AND ACCELERATION

Prepared by

John F. Mahoney
Julius Perel
Bernard E. Kalensher

March 1978

Work Performed Under
AFOSR Contract F44620-75-C-0056

PHRASOR TECHNOLOGY
1536 Highland Avenue
Duarte, California 91010

UNCLASSIFIED

SECURITY CLASSIFICATION OF THIS PAGE (When Data Entered)

REPORT DOCUMENTATION PAGE

READ INSTRUCTIONS BEFORE COMPLETING FORM

1. REPORT NUMBER: AFOSR-TR-78-1026	2. GOVT ACCESSION NO.
3. RECIPIENT'S CATALOG NUMBER	
4. TITLE (and Subtitle): MECHANISMS OF EMITTER SURFACE DAMAGE DURING ELECTROHYDRODYNAMIC COLLOID PARTICLE GENERATION AND ACCELERATION	5. TYPE OF REPORT & PERIOD COVERED: FINAL rept. 1 Feb 76 - 31 Jan 1978
6. PERFORMING ORG. REPORT NUMBER	
7. AUTHOR(s): JOHN F. MAHONEY, JULIUS PEREL, BERNARD E. KALENSHER	8. CONTRACT OR GRANT NUMBER(s): F44620-75-C-0056
9. PERFORMING ORGANIZATION NAME AND ADDRESS: PHRASOR TECHNOLOGY, 1536 HIGHLAND AVENUE, DUARTE, CA 91010	10. PROGRAM ELEMENT, PROJECT, TASK AREA & WORK UNIT NUMBERS: 2308C1, 61102F
11. CONTROLLING OFFICE NAME AND ADDRESS: AIR FORCE OFFICE OF SCIENTIFIC RESEARCH/NA, BLDG 410, BOLLING AIR FORCE BASE, D. C. 20332	12. REPORT DATE: March 1978
	13. NUMBER OF PAGES: 87 (12) 91 p.
14. MONITORING AGENCY NAME & ADDRESS (if different from Controlling Office)	15. SECURITY CLASS. (of this report): UNCLASSIFIED
	15a. DECLASSIFICATION/DOWNGRADING SCHEDULE

16. DISTRIBUTION STATEMENT (of this Report)

Approved for public release; distribution unlimited

17. DISTRIBUTION STATEMENT (of the abstract entered in Block 20, if different from Report)

18. SUPPLEMENTARY NOTES

19. KEY WORDS (Continue on reverse side if necessary and identify by block number)

COLLOID THRUSTER
ELECTRIC PROPULSION
NEGATIVE ION
SPUTTERING
PARTICLE DISTRIBUTION
ELECTROHYDRODYNAMICS
DROPLET PROPERTIES
CHARGED DROPLETS
PARTICLE COLLISIONS

20. ABSTRACT (Continue on reverse side if necessary and identify by block number)

Investigations were directed toward the understanding of the basic colloid thruster generation and acceleration process and the cause of performance degradation. This thruster is applicable for attitude control and station-keeping on future Air Force satellite missions. A theoretical investigation was made of the process of droplet emission to determine the source of negative ion production causing sputter erosion of the emitter. A model of emitter tip erosion has been developed that correlates with performance degradation. The erosion is caused by back bombardment of the emitter by negative

DD FORM 1 JAN 73 1473 EDITION OF 1 NOV 65 IS OBSOLETE

391 701

UNCLASSIFIED

SECURITY CLASSIFICATION OF THIS PAGE (When Data Entered)

ions produced from the breakup of slow droplets as a result of collisions with fast ions. Calculations were initially made assuming the droplets were all the same size. If at least one negative ion is produced to each ion/droplet collision, the resulting sputtering rate is sufficient to explain the measured erosion. A distribution of droplet sizes also included in the analysis shows that the calculated collision ratio increases when the droplet population is changed to the assumed distribution. Consequences of varying the distribution were examined. Recommendations are made to eliminate or decrease the erosion. New insight into droplet properties and collision processes was obtained through this investigation.

FOREWORD

This report was prepared by Phrasor Technology of Pasadena, California, under Air Force Contract F44620-75-C-0056, project and task numbers 2308C1 and 61102F. This report covers the period from February 1975 to January 1978.

The research is supported by the Air Force Office of Scientific Research, and the program monitored by Dr. B. T. Wolfson, NA.

This report describes the considerations and results in developing analytical models of colloid thruster emitter operation and erosion. An earlier and preliminary report on this work was presented at the AIAA 12th Electric Propulsion Conference (Ref. 1).

This technical report has been reviewed and is approved.

ABSTRACT

This program was directed toward the understanding of the basic colloid thruster generation and acceleration process and the cause of performance degradation. This thruster is applicable for attitude control and stationkeeping on future Air Force satellite missions. A theoretical investigation was made of the process of droplet emission to determine the source of negative ion production causing sputter erosion of the emitter. A model of emitter tip erosion has been developed that correlates with performance degradation. The erosion is caused by back bombardment of the emitter by negative ions produced from the breakup of flow droplets as a result of collisions with fast ions. The calculations were initially made by assuming that the droplets were all the same size rather than using the distribution of droplet sizes actually observed. If at least one negative ion is produced at each ion/droplet collision, the resulting sputtering rate is sufficient to explain the measured erosion. A distribution of droplet sizes was also included in the analysis which consisted of a normal distribution of the charge-to-mass ratios. Results of the analysis show that the calculated collision ratio increases slightly when the droplet population is changed slightly from uniform size to the assumed distribution. The consequence of varying the distribution were examined by changing the standard deviation and by replacing the normal distribution by an unsymmetrical distribution. Recommendations are made to eliminate or decrease the erosion through changing thruster operational parameters. In addition, new insight into droplet properties and collision processes was obtained through this investigation.

CONTENTS

CONTENTS (contd)

ILLUSTRATIONS

SECTION 1

INTRODUCTION

Colloid thrusters having multiple needle emitters experience degradation in performance after thousands of hours of operation. This was attributed to the change in the electric field at the emitter tip caused by erosion which occurred during that period of operation.

This report describes the development of an analytical model for understanding the collision processes in the colloid thruster exhaust beam and emitter erosion mechanisms.[1] Erosion or surface damage by sputtering mechanisms is considered to be the cause of performance degradation. Other erosive (or corrosive) mechanisms were considered initially as possibly being responsible for the damage in the EHD spraying process, but sputtering was determined to be the primary cause for producing most of the surface damage.

The technical approach taken initially in this study was to consider particle interactions and formulate simplified models involving particle collisions. This approach was used for the purpose of gaining physical insight into the interaction process which was then applied to expanded models involving more complex analyses.

The guidelines for the calculations presented in this report were obtained from needle erosion rates and data. Many of the values for parameters used in the theoretical development were derived from TRW thruster module operational data.

Initially, diffierent regions in the thruster and vacuum chamber were examined, along with other mechanisms, to determine the cause of the erosion. The emphasis for study was chosen to be the acceleration

region, near the droplet emitter. This region was chosen for investigation for two reasons. First, the particle densities, with the possible exception of electrons, are highest here and are decreasing functions with distance from the emitter. Second, negative particles, suspected as a primary cause of sputter erosion if formed as a result of collisions in the acceleration region, are not generally able to escape the region and can readily bombard the emitter surface.

The charged droplet beam generated by colloid thrusters consists of a distribution of particle sizes covering a range from molecular ions to larger droplets containing as many as 10^5 molecules/droplet. Initially, this distribution was supplanted by a typical particle taken as the mean charge-to-mass ratio. This droplet has a radius of 50Å and a mean specific charge of 10^4 C/kg. Many aspects of thruster beam interaction collisions using this single particle model do not differ greatly from results obtained by taking the actual particle distributions into account. This was verified by extending the single particle model to include charged particle distribution functions.

The analysis, made in consideration of the dynamic and static conditions occurring in the operation of colloid thruster, supports the erosion model presented. The model involves the collision of positive ions and droplets both generated at the emitter and the subsequent breakup of the droplets. Among the fragments produced by the breakup of each droplet, only one negative ion (probably that of iodine used as the propellant dopant) is required to explain the measured erosion. The negative ion is accelerated toward the emitter hitting only exposed surfaces to form the observed erosion.

As a result of the analysis, recommendations are made to eliminate, or at least minimize, the erosion through changing thruster operational parameters. A summary of the erosion model resulting from this program is given in subsection 7.1, which is recommended for review.

SECTION 2

THRUSTER EMITTER DYNAMICS

2.1 PERFORMANCE DEGRADATION AND EROSION

Colloid charged particle generation was easily accomplished in the initial stages of the research, but the control and understanding of the fundamental physical processes involved proved a more difficult task. The development of colloid thrusters has proceeded primarily by empirical investigations without sufficient and practical theoretical models to describe the interdependence of such thruster variables as thrust, specific impulse, and specific charge of efficiency.

Duration tests of colloid thruster modules at TRW, Inc., show degradation in performance after only several thousand hours of operation. Examination of the emitters revealed some form of erosive attack at the capillary needle edges.[2] The performance degradation measured in terms of decreasing specific impulse has been attributed to this damage. The damage is thought to be material sputtering erosion caused by negative particle bombardment. However, because of the extraordinary conditions at the emitter tips, other surface damage mechanisms may be active which would not be anticipated in a less extreme environment. Data from long term operation of emitters reveal erosion that occurs at the rate of about one mil in a year. The emitter tip geometry is apparently altered sufficiently to modify the electric field in the emission areas and thereby decrease the specific impulse. Performance can be restored by increasing the high voltage applied to the emitters, but this does not completely restore the local electric field to reproduce the desired operation. A somewhat different operating mode is thereby achieved in which degradation may be accelerated, in addition to other unwanted effects such as changes in the beam spread and beam distributions.

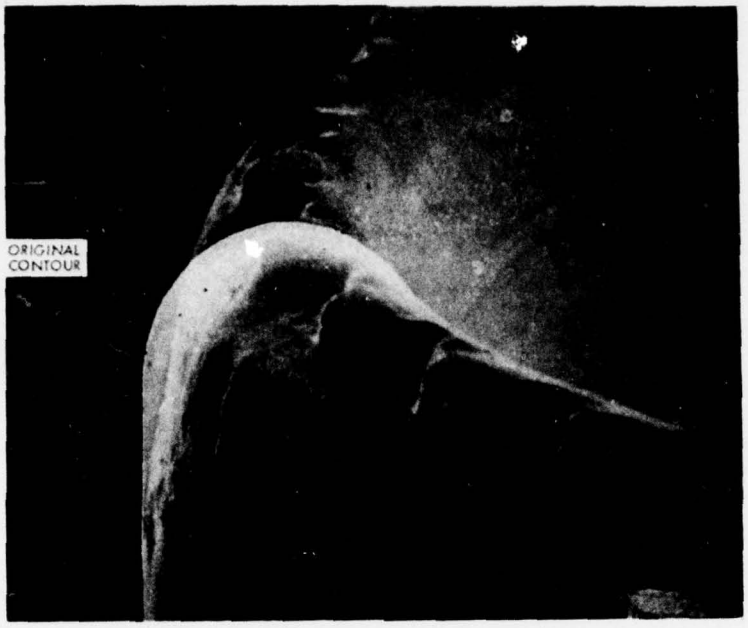

Figure 1. Eroded Needle

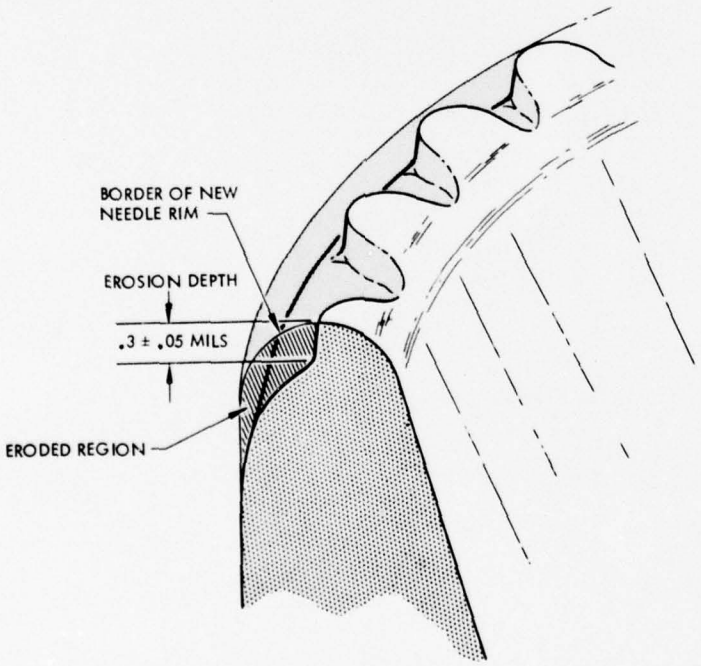

Figure 2. Eroded Area of Needle

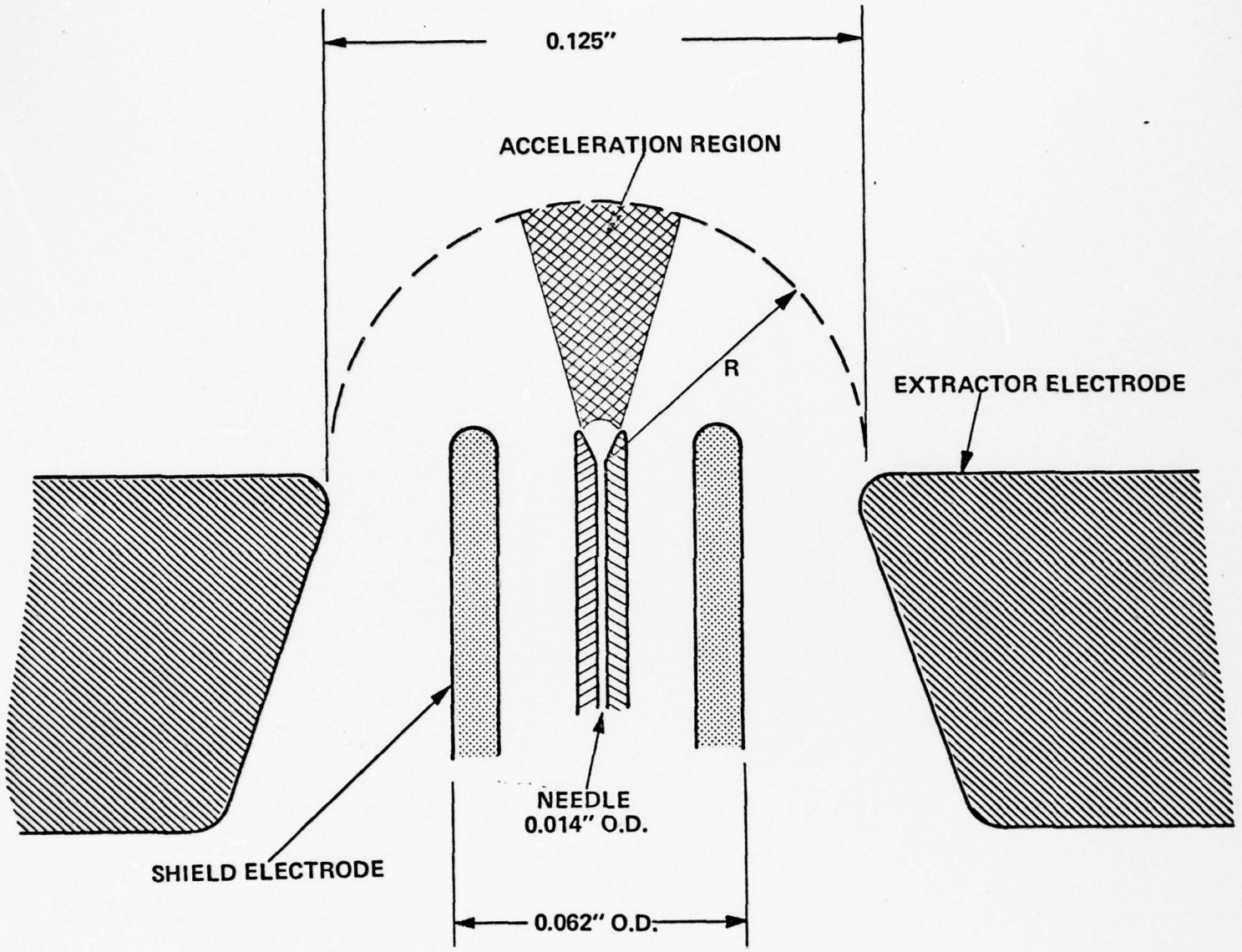

Figure 3. *TRW Needle Geometry Showing Interaction Region Considered for Collisional Studies*

A photograph made by TRW, Inc., showing the typical pattern of emitter damage is shown in Figure 1 (Ref. 2). The individual sites for jet formation can be observed, along with marks due to machining made during the emitter fabrication. The rims are eroded only on the outside, indicating that attack by electrolytic action is not prevelant. The physical evidence of erosion on the rims and outside needle diameter suggests the damage is caused by negative ion sputtering with the scalloped mounds protected by the liquid jets. Figure 2 illustrates the eroded area of the needle, showing significant dimensions. The results from one-dimensional modeling of the interaction phenomenon in the colloid exhaust plume is advanced as an explanation for the erosive damage to colloid thruster emitters.

2.2 THE ACCELERATION REGION

The most important area of interest in the erosion study is the acceleration region in the vicinity of the emitter tip. Figure 3 depicts the TRW needle geometry showing the acceleration region, or region of interaction, under consideration for particle collisions in the sputtering studies. The needle emitter has a 0.014 inch outer diameter and a 0.005 inch inner diameter and is constructed from a platinum (90%)/iridium (10%) tubing. The needle is surrounded by a concentric cylindrical shield having a 0.062 inch outer diameter. The shield/emitter assembly is centered in a planar extractor electrode which has a 1/8 inch aperture.

The acceleration region in Figure 3 extends from the needle emitter tip to a distance approximately equal to the radius of the extractor aperture. It includes the particle beam, diverging from the emitter, and the intense electric field.

The Potential Function

An analytical expression for the potential distribution arising from the electric fields in the region of the emitter and extractor electrodes was formulated. The potential function is required for calculations of charged particle density functions, cross sections, and other analyses involving charged particles. The required distribution function would be ideally derived from the boundary conditions implied in electrode geometry shown in Figure 3 and also include the effects of space charge. A potential function found to be adequate for much of the quantitative analyses in this report is given below:[3]

$$V(x) = \frac{V_o \ \ell n\left(\frac{R}{x + \frac{1}{2} r_o}\right)}{\ell n\left(\frac{2R}{r_o}\right)} \qquad (1)$$

This expression was derived by considering a tip geometry of parabolic shape surrounded by a grounded surface having a parabolic shape, where $V(x)$ and V_o are the potentials at a distance, x, from the emitter and at the emitter surface, respectively. The distance between the tip and the grounded surface given by R and r_o is the radius of curvature at the tip. For application of Eq. (1) to the emitter geometry, R is taken as the radius of the extractor electrode aperture and r_o as the radius of the needle emitter. For the case where a needle emitter is surrounded by a shield electrode, shown in Figure 3, r_o is taken as the radius of the shield electrode. The potential calculated using Eq. (1) falls to a value of zero at a distance, R, along the emitter axis, equivalent to the extractor aperture radius. The value of r_o determines the rate at which the field decreases with distance. Values for the potential distribution were calculated for the geometry used for computer generated field plots supplied by TRW, Inc.[4] The results are shown in Figure 4, where curve A was calculated from the

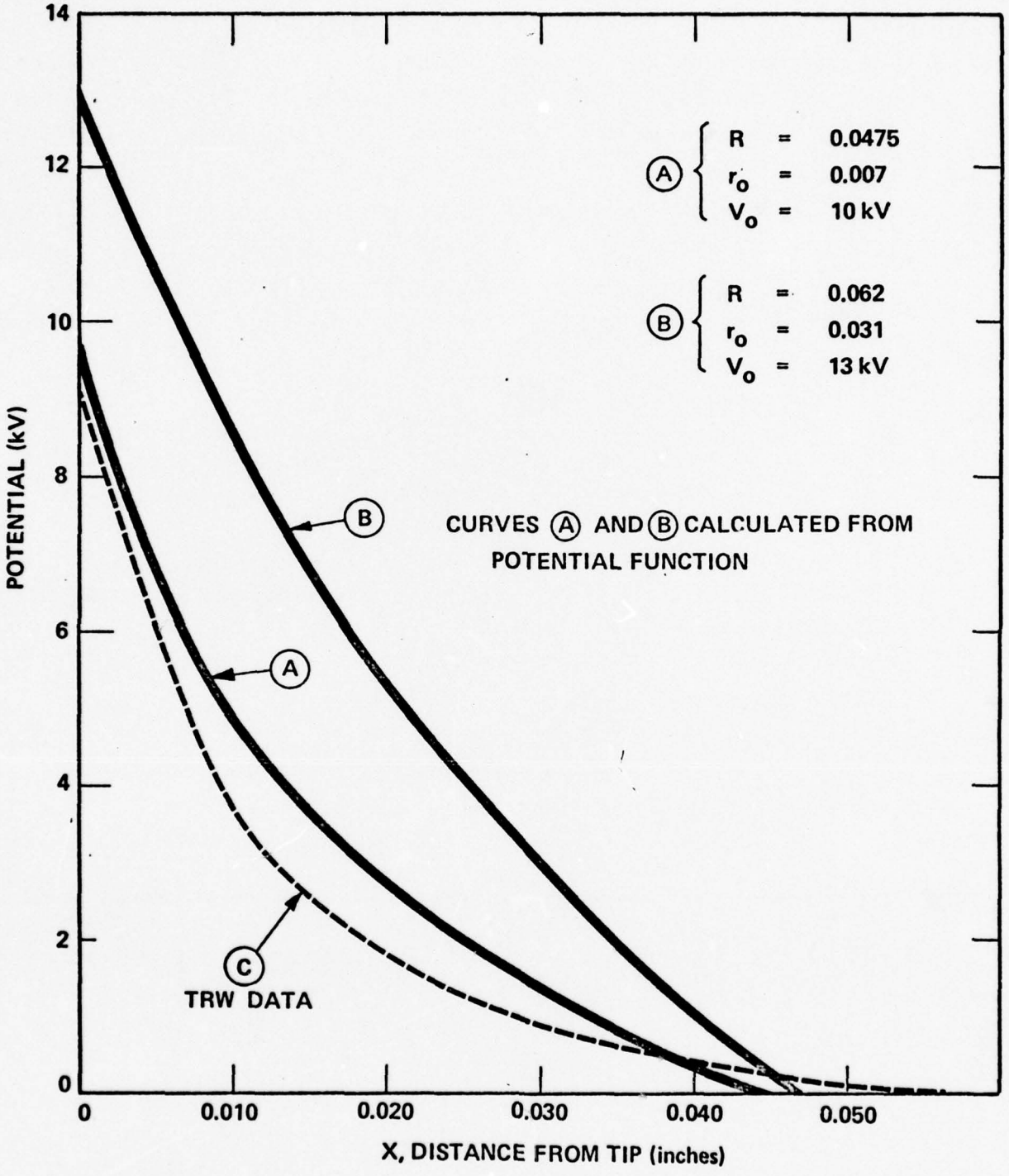

Figure 4. Potential as a Function of Distance from Emitter Surface

potential function (Eq. 1) and curve C was obtained from the computer studies. The differences between the computer data and calculations can be seen from examination of Figure 4. At $x = R - 1/2\ r_o$, the potential functions goes to zero, whereas the computer values extend slightly beyond R. Compared with the analytic expression, the computer potential shows a more rapid decrease as a function of distance from the emitter tip. Curve B is a plot of Eq. (1) for the geometry where erosion data are not available. The needle voltage is assumed to be 13 kV, and r_o is the radius of the shield equal to 0.031 inch. Note in Curve B that the field does not drop off as rapidly in the vicintiy of the emitter tip as a result of the presence of the shield electrode.

2.3 SPUTTERING AS A MECHANISM

Emitter surface sputtering rates are examined which can account for the loss of material observed experimentally during long-term operation of colloid thrusters. For every ion that bombards a surface, S atoms are sputtered off the surface, where S is no more than an order of magnitude from unity for the species and energies involved here.

The bombarding ion current, I, necessary to sputter a mass, m, of target material is given by the relation:

$$I(\text{ions/sec}) = \frac{1.66 \times 10^{14}\ V_s \rho}{A\ S\ t},$$

where, V_s is the sputtered volume, ρ the density of the material (μg/unit volume), A is the mass number of the target atom, S is the sputtering yield (a oms/ion), and t is the bombardment time in hours.

In order to calculate the incident ion bombardment rate at colloid emitters that could cause erosion, assuming various sputtering yields,

published erosion rates for the needle emitters tested at TRW were used.[5] Assuming a 0.001 inch thickness for the needle rims and an erosion rate of 1 mil/year, the following incident negative ion rates were calculated:

Sputtering Yield S (atoms/ion)	Incident Ion Rate I (ions/sec)
1	1.39×10^9
5	2.78×10^8
10	1.39×10^8

Bombardment rates on the order of 10^8 to 10^9 ions/sec could account for the observed erosion rates. Sputtering yields in the range from 1 to 10 atoms/ion are possible if the bombarding species is assumed to be negative iodine ions or large negative cluster ions. To our knowledge, there are no data available on the sputtering yields for negative iodine atoms incident on a platinum target. A crude approximation for the sputtering yields involving iodine ions can be made by extrapolating data and theory for other species incident on platinum. Figure 5 shows a plot of sputtering rates for argon ions on platinum over the energy range 1 to 13 kV. The argon yield curve, denoted by $S(A^+)$ was constructed using a universal yield-energy relation for argon ion bombardment on various solid targets.[6] The upper curve in Figure 5 is the estimated sputtering ratio for iodine ions incident on platinum denoted by $S(A+)$ (M_1/M_2). This curve was constructed from the argon curve assuming that sputtering yields on a given target by various ion species is directly proportional to the mass of the incident ion. This was obtained by multiplying the sputtering ratios for argon by the ratio of the iodine to argon ion masses which is 3.14. The resultant yield curve for iodine is believed to overestimate the sputtering ratio, and the more realistic sputtering ratios probably fall between the argon and the estimated iodine yield curves. Therefore, it is not unreasonable to assume that iodine ions could sputter as many as

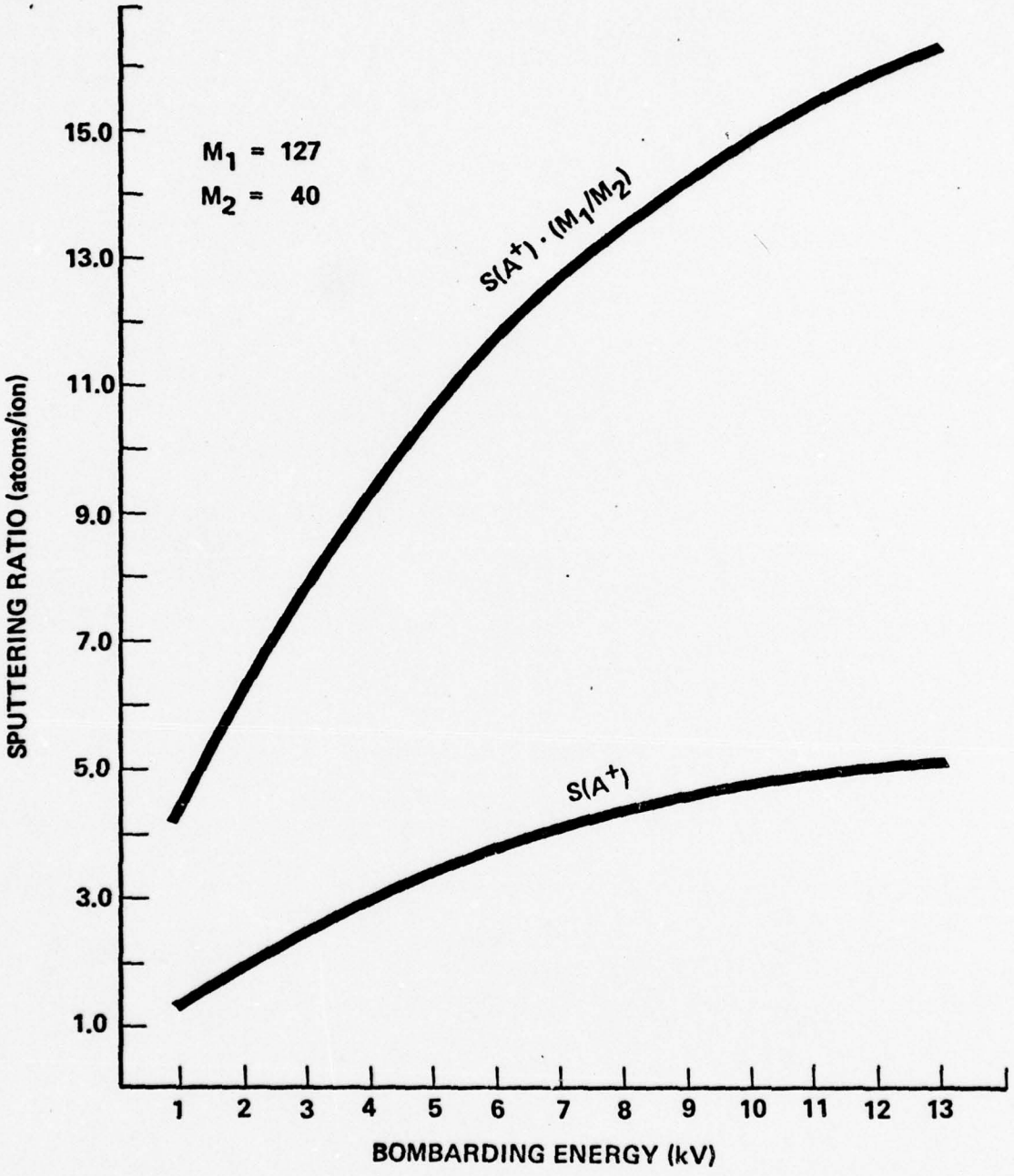

Figure 5. Sputtering Ratio for Iodine Ions Incident on Platinum Target Estimated from Argon Ion Yields

10 surface platinum atoms percollision for the energy range considered. If negative ions of the type OH^- or negatively charged glycerol fragment ions are also contributing to the erosion of emitters, they are not expected to produce high sputtering yields similar to iodine, since their masses are much smaller.

SECTION 3

PARTICLE SPECIES IN EXHAUST BEAM ACCELERATION REGION

Before collision rates and cross section analyses can be undertaken, determinations will be made on particle species populating the exhaust beam and their corresponding density functions. The particles most likely involved in beam collision processes are thermally evaporated neutral glycerol molecules, EHD generated molecular ions and charged droplets, and, finally, electrons. With the exception of the latter, approximate density functions can be determined with some knowledge of the generating mechanisms producing the particles. Since, in this analysis, we are not concerned with particle densities outside the accelerating region, variations in charged specie densities will be due to particle accelerations and beam divergence. The density function for neutral glycerol molecules was calculated starting with a conventional cosine distribution.

3.1 THERMALLY EVAPORATED NEUTRAL GLYCEROL MOLECULES

The number of molecules per square centimeter per second (J) passing a unit area per unit time at a distance, r, from a source whose area is A is:

$$J = \frac{\rho_o \bar{v}_o A \cos\theta}{4 \pi r^2}, \qquad (2)$$

where ρ_o is the number of molecules per cubic centimeter at the source and $\bar{v}_o$ is the mean velocity of the molecules.[7] Equation (2) applies when r is large compared with the dimensions of the source. In the accelerating region, distances are not large compared to the needle dimensions. A point source approximation such as Eq. (2) is not valid for accurate determinations of the density of thermal glycerol molecules in close proximity to the evaporating surface of the propellant

fluid. The problem of an extended effusive source was solved for the special case of determining the number of density along the colloid emitter axis perpendicular to the emitter surface ($\theta = 0^{o}$). The result is given by:

$$J(x) = \tfrac{1}{4}\rho_o \bar{v}_o \left(\frac{r_o^2}{x^2 + r_o^2}\right) = \tfrac{1}{4} \rho_o v_o f(x) \ (mol/cm^2\text{-}sec) \qquad (3)$$

where x is the distance along the emitter axis and r_o is the radius of the emitter. At $x = 0$, the expression for $J(x)$ reduces to $\frac{1}{4} v_o$, where ρ_o is the density at the surface and $\bar{v}_o$ is the mean thermal velocity. When x is large compared with r_o and for the case $\theta = 0^{o}$, Eq. (3) reduces to

$$J(x) = \tfrac{1}{4} \rho_o \bar{v}_o \left(\frac{r_o^2}{x^2}\right), \qquad (4)$$

which is identical to Eq. (2) for a source having circular dimensions of πr_o^2. A normalized form of Eq. (3), i.e., $f(x)$ is graphically displayed as a function of distance from the source, x, in units of x/r_o in Figure 6. For comparative purposes, the point source approximation given by Eq. (4) is also plotted. At large distances from the emitter, the extended source solution can be seen to approach the point source formulation. When x is small, the point source solution diverges to infinity while the normalized flux approaches unity. Note that, at a distance of $x = 10\ r_o$, the particle density will have decreased by a factor of 100.

The neutral glycerol molecular density as a function of x is defined as:

$$\rho(x) = J(x)/\bar{v}_o$$

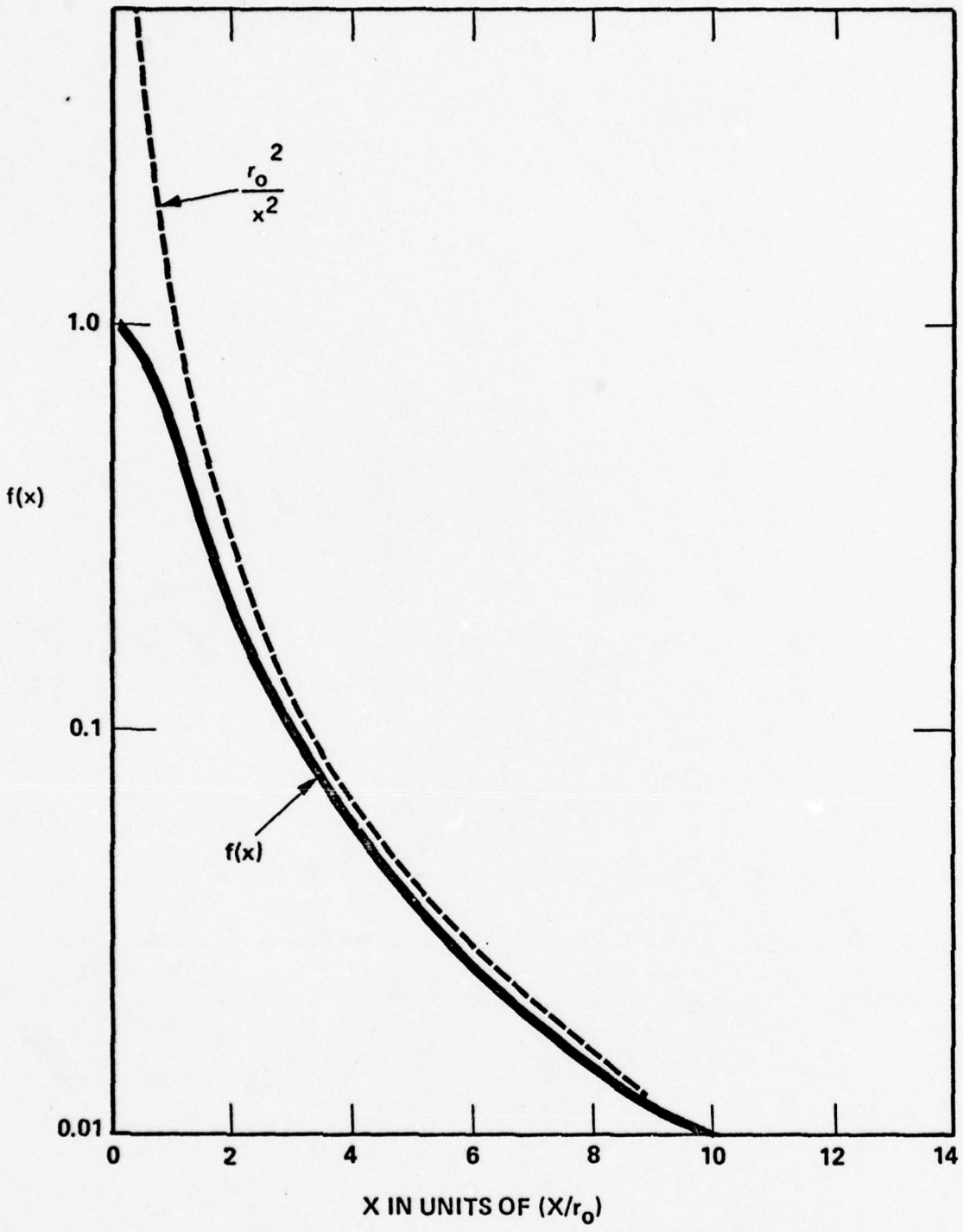

Figure 6. Thermal Particle Density as a Function of Distance from Source

By substitution of Eq. (3) into the above, the density function becomes

$$\rho(x) = \frac{J_o}{\bar{v}_o}\left(\frac{r_o^2}{x^2 + r_o^2}\right), \tag{5}$$

where J_o, the rate of evaporation of molecules per square centimeter per second, is $\frac{1}{4}\rho_o\bar{v}_o$ and is calculated from Reference 8.

$$J_o = 3.64 \times 10^{21} P_v/T^{\frac{1}{2}} \text{ (mol/cm}^2\text{-sec)}, \tag{6}$$

where P_v is the vapor pressure of glycerol in units of torr, at the absolute temperature, T. The velocity $\bar{v}_o$ is given by

$$\bar{v}_o = \left(\frac{8\ kT}{\pi m}\right)^{\frac{1}{2}}, \tag{7}$$

where k is the Boltzmann constant and m is the mass of the molecule. It is useful to note that the vacuum evaporation rates of glycerol have been experimentally measured at a background pressure of 5×10^{-6} torr.[9] The results of these measurements show that the observed evaporation rates of glycerol were found to be less than the maximum calculated rates for J_o given by Eq. (6). A vaporization coefficient α_v given by

$$\alpha_v = J'/J_o,$$

is used to indicate the ratio of the observed J' to the calculated rates of evaporation which, for glycerol, has the value of 0.34. Since the observed rate of evaporation is nearly one-third that of the calculated rates, α_v should be incorprated into Eq. (5) so that

$$\rho(x) = \frac{\alpha_v J_o}{\bar{v}_o}\left(\frac{r_o^2}{x^2 + r_o^2}\right). \tag{8}$$

Variations in the density of thermal glycerol molecules in the accelerating region can be calculated using Eq. (8), remembering that J_o and $\bar{v}_o$ are temperature dependent. At a temperature of 20°C, the vapor pressure of glycerol is 1.7×10^{-4} torr. The calculated value of J_o from Eq. (6) is given by 3.7×10^{16} mol/cm^2-sec. Using this value and the velocity given by Eq. (7), the neutral glycerine molecular density given by Eq. (8), at a distance of 8.75 mils, is given by 2×10^{11} mol/cm^3. At 10 emitter radii, the density drops to about 2×10^9 mol/cm^3 and decreases rapidly with greater distance.

3.2 MOLECULAR ION CURRENT DENSITIES

Molecular ions are defined as any cluster composed of glycerol molecules that carry a single electronic charge. The existence of molecular ions is evidenced by the peaks occurring in the initial portion of time-of-flight waveforms, and they have also been detected using EH ionization mass spectrometry techniques employed to measure the ionization of glycerol from needle emitters.[10] In the latter study, singly charged ions containing up to eight glycerol molecules were observed. The charge associated with the molecules of the form $[G_n + Na]^+$ for n from 0 to 8 was attributed to the Na^+ ion. During typical operation of a colloid needle emitter, 10 percent of the total needle current can be attributed to ion emission.

Data taken from Reference 10 was combined with the ion peak normally observed in time-of-flight (TOF) curves to produce Figure 7. The dashed line is a typical ion peak in TOF data with the total ion current plotted on an arbitrary scale of 100. The different molecular ion fragments taken from Reference 10 were plotted as vertical lines at the time-of-flight for the arrival of such ions as Na^+, $G + Na^+$ (where G represents a glycerine molecule), etc. Since the TOF data have a relatively long time constant, the scope trace was not able to

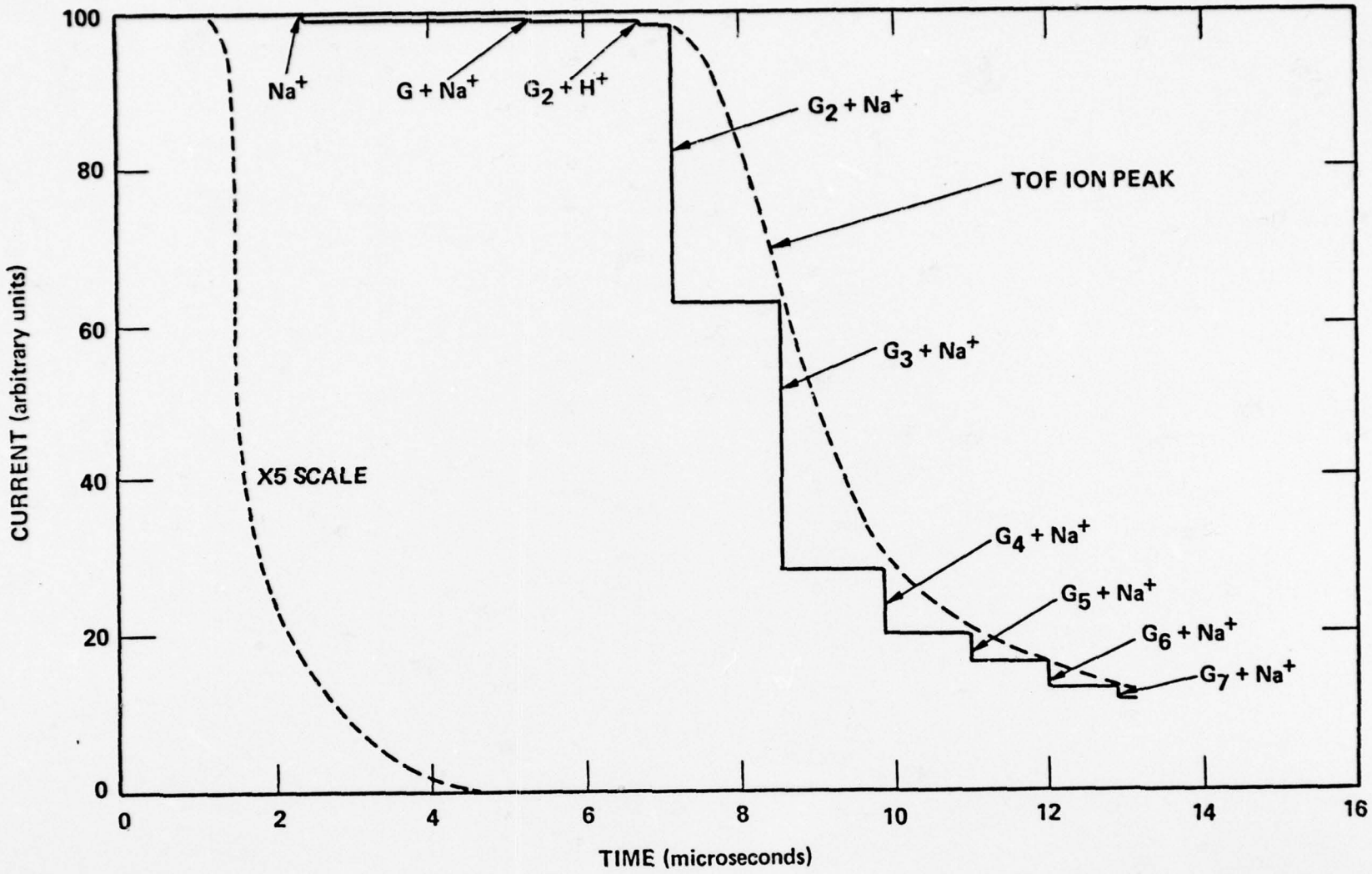

Figure 7. TOF Construction of Ion Peak Using EHD Mass Spectrometry Data

follow the sharp steps shown with the continuous line but showed the decay seen in the dashed line. The correlation of these two data verify the existence of these various ion fragments in the colloid beam.

The emission rate of ions can be calculated from

$$\upsilon = I_{ion}/q$$

where I_{ion} is that portion of the needle current attributed to ion emission and q is the charge of the ion equivalent to 1.6×10^{-19} coulomb. Assuming a total needle current of 10 μA, I_{ion} is then 1 μA, and molecular ion emission rates are calculated to be approximately 6×10^{12} ions/sec. It is interesting to note that ion emission rates are of the same order of magnitude as droplet emission rates to be discussed next.

3.3 CHARGED DROPLETS

A number density for a charged droplet of given size in the accelerating region can be calculated from the particle generation rate at the emitter. The charged particle flux Ø, in droplets per second per unit area, is determined from $\emptyset = \upsilon/A_r$ where A_r is the emission area at the surface of the emitter and υ is the emission rate in droplets per second. Assuming the colloid beam consists of particles having uniform size determined from the mean charge-to-mass ratio of the distribution, a characteristic frequency for this particle over the entire emitter is defined as

$$\upsilon = I_t/q, \tag{9}$$

where I_t is the total needle current and q is the charge carried by the mean specific charge particle. Applying Rayleigh's criteria determines the charge (q) for the mean specific charge particle for glycerol and the characteristic emission frequency becomes

$$\upsilon = 1.49 \times 10^{13} I_t \langle C \rangle ,$$

where $\langle C \rangle$ is the mean specific charge characterizing the distribution. For a mean specific charge of 10^4C/kg and I_t of 10 μA, $\nu = 1.49 \times 10^{12}$ droplets/second. The mean specific charge is given by $\langle C \rangle = I_t/\dot{m}$, where $\dot{m}$ is generally one μg/sec and I_t is given above. This results in the value of 10^4C/kg.

The charged particle flux density in the accelerating region is given by the continuity relationship as

$$\emptyset = \rho(x)\, v(x) \tag{10}$$

The velocity $v(x)$ of the droplet is not constant because of the accelerating forces and varies according to

$$v(x) = 2C[V_o - V(x)]^{\frac{1}{2}}, \tag{11}$$

where V_o and $V(x)$ are the potentials at the emitter surface and at a distance x from the emitter, respectively. Assuming $\rho(x)\, v(x)$ to be constant neglects any divergence due to off-axis particle emission and space charge spreading. Combining Eqs. (10) and (11), the droplet density function becomes

$$\rho(x) = \emptyset \left\{ 2\, C\, [V_o - V(x)]^{\frac{1}{2}} \right\}^{-1} \tag{12}$$

Note that V(x) is the potential function in Eq. (1) of Section 2. This solution for the density function will diverge in the limiting case at $x = 0$ where the velocity approaches zero and $\rho(x) \rightarrow \infty$. This situation is commonly encountered in problems of space charge limited currents.

The droplet density function as a function of distance from the emitter taken from Eq. (12) is shown in figure 8. For this plot $\langle C \rangle$ was taken as 10^4 C/kg, I_t as 10 μA, V_o as 13 kV, and the standard geometry shown in figure 3 was used to calculate values for the potential function. As

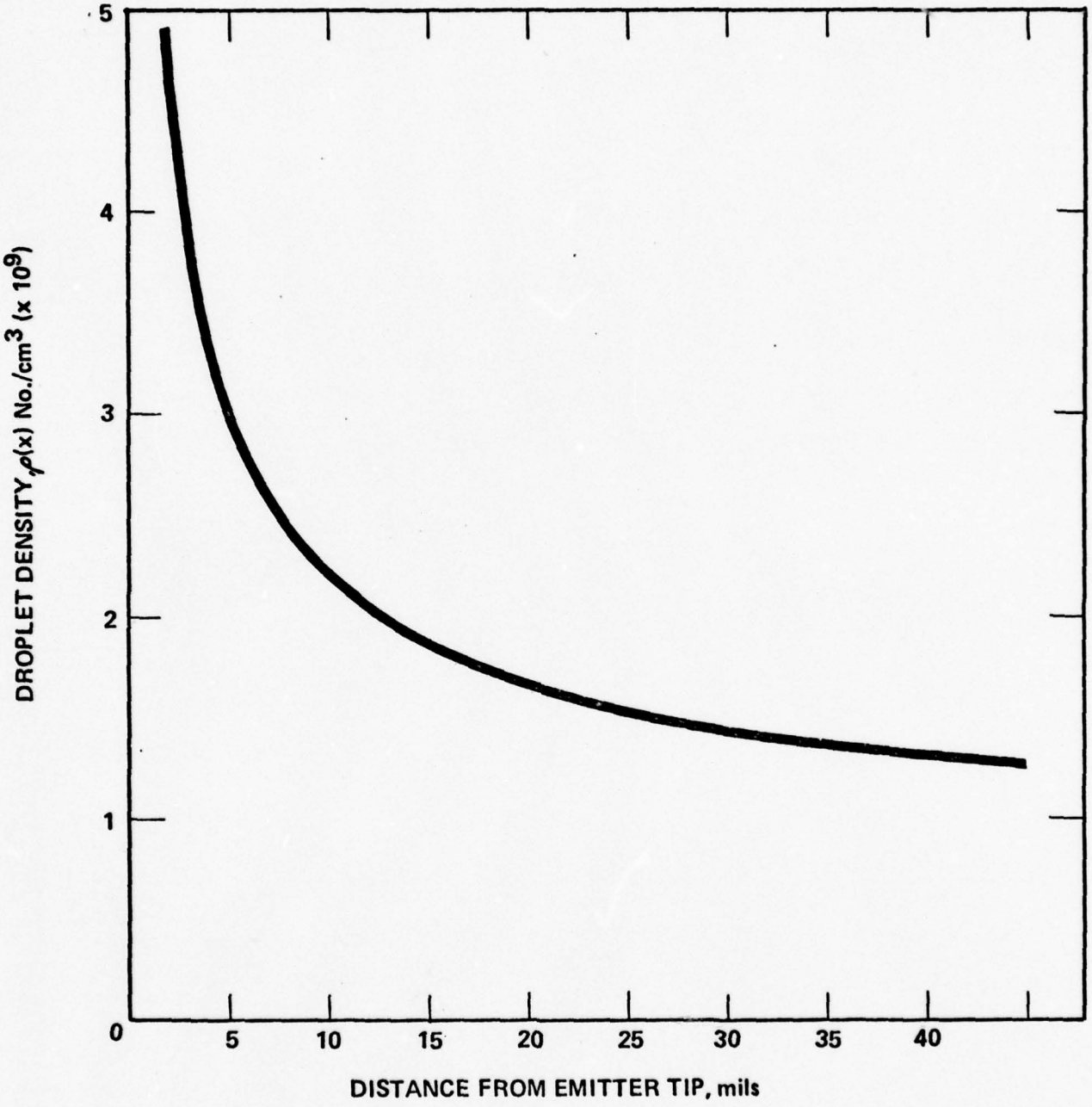

Figure 8. Droplet Density as a Function of Distance from Emitter Tip
V_o = 13 kV

seen in the figure, droplet densities are on the order of 10^9 per cubic centimeter in the accelerating region. Because of the space charge divergence, the density will decrease more rapidly than indicated here.

3.4 STRUCTURE AND ENERGETICS OF CHARGED DROPLETS

The charged droplet distribution represented by the mean specific charge of 10^4 C/kg has a significant role in the collision studies. The prediction of collision products after a droplet is bombarded by another particle requires some knowledge of the structure and energy of the droplet. An examination of particle properties including a discussion of particle stability and energetics will be made and subsequently applied to collision analyses in the next section.

3.4.1 DROPLET PROPERTIES

Table I lists some typical properties of a droplet assumed spherical in shape. The droplet mass, charge, and radius were determined from Rayleigh's criteria for a specific charge of 10^4 C/kg. The ratio of glycerol molecules to sodium iodide molecules was calculated for a solution of 20 grams NaI dissolved in 100 ml of glycerol. The ratio was then used to determine the number of glycerol and NaI molecules in the droplet from the following relationships:

$$N_g = \frac{M_D}{(m_g + m_{NaI}/R)} \tag{13}$$

and

$$N_{NaI} = \frac{M_D}{(Rm_g + m_{NaI})} , \tag{14}$$

where m_g and m_{NaI} are the masses of the glycerol and NaI molecules in grams, M_D is the mass of the droplet, and R is the ratio of glycerol to NaI molecules.

TABLE I

DROPLET PROPERTIES

Charge-to-Mass Ratio	10^4 C/kg
Radius	50Å
Charge	+40e
Mass	6.67×10^{-22} kg
Number of Glycerol Molecules	3.74×10^3
Number of NaI Molecules	3.7×10^2
Number of Surface Molecules	10^3
Glycerol/NaI Molecule Ratio	10:1
Emission Frequency	10^{10} - 10^{11} drops/sec
Surface Area	3.14×10^{-12} cm^2
Volume	5.24×10^{-19} cm^3
Geometric Cross Section	7.85×10^{-13} cm^2

Although dissolved iodine atoms contribute little to the mass of the droplet, their presence in the droplet may be a key factor in the production of negative ions during droplet breakup or evaporative collisions (see Section 6). The droplet emission frequency of 10^{10} to $1o^{11}$ drops/sec was estimated from the characteristic frequency derived previously. The frequency in Table I represents the rate of droplet emission from a single spraying site and implies a number of individual spraying sites between 10 and 100. Evidence that 30 to 40 spraying sites are active during operation of needle emitters was seen in scanning electron photomicrographs, Figure 1.[5] A frequency spectrum constructed from time-of-flight waveform supplied by TRW shows that a particle of mean specific charge of 10^4 C/kg has an emission frequency ($\Delta I/q$) in the range 10^{10} to 10^{11} drops/second.

The stability of a charged droplet generated in the EHD spraying process will depend to a large extent on the intermolecular forces of attraction

acting between individual molecules in the droplet. These forces, as shall be seen later, which are described by Van der Waals dipole and dipole-induced interactions, are not particularly strong compared with intramolecular covalent or ionic bonds. Further, the cohesive stability of a charged droplet is lessened by the electrostatic repulsion energy due to excess charge and also by elevated temperatures arising from I^2R heating during the droplet formation process.

3.4.2 ENERGETICS OF AN UNCHARGED DROPLET

Insight into the stabibility of a charged liquid droplet can be gained by considering the various energy states of a molecule residing in an uncharged droplet. The energy level diagram for a liquid droplet is shown in Figure 9, and the following terms are defined in reference to the figure:

E_s = absolute energy of molecule on surface of droplet

E_L = absolute energy of molecule in the interior of droplet (cohesive energy) in normal, bound state

E_F = energy state of unbound, free molecule

ϵ_s = surface energy - energy required to bring molecule from interior of droplet to the surface

E_t = total energy of all molecules in droplet occupying surface and interior states

The total cohesive energy of all molecules in the droplet is the sum of the energies of the molecules in the droplet interior and the molecules on the surface:

$$E_t = (N_t - N_s)\, E_L + N_s\, E_s \qquad (15)$$

where N_t and N_s are the total number of molecules in the droplet and the number of molecules on the surface, respectively. Rearrangement

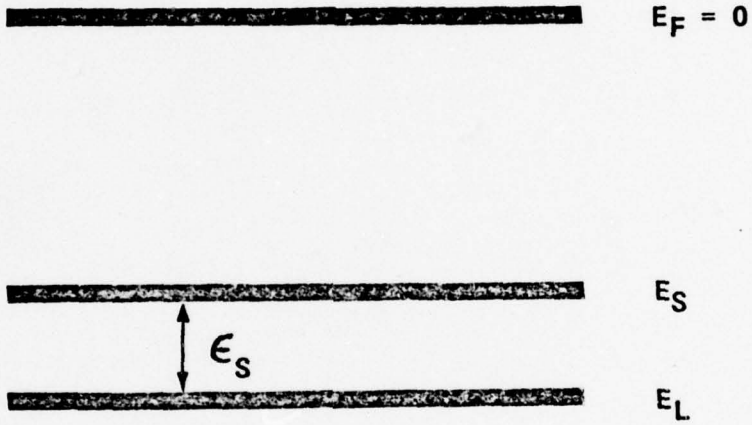

Figure 9. Liquid Droplet Energy Diagram

of the terms in Eq. (15) yields:

$$E_t = N_t E_L - N_s (E_L - E_s) \tag{16}$$

From the energy diagram, $E_L - E_s = \epsilon_s$ and ϵ_s can be replaced by $\frac{\gamma A}{N_s}$, where γ is the surface energy and A is the surface area of the droplet. Making the proper substitutions, the total energy becomes:

$$E_t = N_t E_L - \gamma A \tag{17}$$

Thus, E_t represents the cohesive energy of a droplet whose value can be estimated from the actual heat of vaporization when the substance evaporates into the atomic or molecular constituents. The energy, E_t, can also be interpreted as the energy required to evaporate the droplet into a gas composed of its individual molecules assuming no energy losses in the form of kinetic energy, ionization, excitation, etc.

For the case of a charged droplet, the energy E_t will be less by an amount corresponding to the electrostatic repulsive energy due to the mutual interaction of the net charges residing on the surface of the droplet. The electrostatic energy of a system of charges on the droplet surface whose radius is R and the number of charges is Z can be expressed as:

$$U = \frac{(Ze)^2}{4\pi \epsilon_o R} .$$

The total cohesive energy of a charged droplet becomes

$$E_t = N_t E_L - \left[\gamma A + \frac{(Ze)^2}{4\pi \epsilon_o R} \right] . \tag{18}$$

The following subsection is devoted to a discussion of E_L, the energy of attraction between molecules in a liquid droplet.

3.4.3 INTERMOLECULAR ATTRACTION ENERGIES

To simplify the development of a model for droplet energy, the droplet is treated as though composed of glycerol molecules only. The consequences of neglecting the effects of NaI molecules, I atoms, and Na^+, I^- atomic ions on the total intermolecular binding energy of a droplet will be discussed later. Glycerol molecules possess a permanent dipole moment of 2.68×10^{-18} e.s.u. which is greater than that of water.[11] The forces of attraction acting between glycerol molecules are due in part to its dipole moment. The Van der Waal's intermolecular attraction energy between two identical molecules possessing permanent dipole moments is given by Reference 12.

$$E_L = \frac{1}{r^6}\left(\frac{2\mu^4}{3kT} + 2\mu^2\alpha + \frac{3}{4}\alpha^2 I\right) , \qquad (19)$$

where the interaction distance between the molecules is given by r, μ is the dipole moment, α is the polarizability of the glycerol molecule, k is Boltzmann's constant, T the absolute temperature, and I is the ionization potential of a glycerol molecule. The first term inside the parentheses is the average energy of the dipole-dipole interaction. The second term represents the energy of attraction due to the induced dipole in the first molecule by the field of the permanent dipole of the second molecule, and vice-versa. The last term is the dispersion energy representing a net force due to instantaneous forces of attraction resulting from the appearance of momentary dipoles.

Before E_L, the intermolecular attraction energy between glycerol molecules, can be calculated, the values of the polarizability (α), ionization potential (I), and interaction distance (r) for glycerol

must be estimated. The polarizability of the glycerol molecule was estimated using the relation:

$$\alpha = 3/4 \left(\frac{K - 1}{K + 2}\right) \frac{M}{\pi \rho N} , \qquad (20)$$

where K is the dielectric constant, M is the molecular weight, ρ is the density of the liquid, and N is Avogadro's number.

Using Eq. (20), the polarizability for glycerol was calculated to be 2.72×10^{-23} cm^3, which is the value found in most organic liquids.[13] In general, the polarizability tends to increase with increasing size of the molecule. Thus, in calculating the polarizability of glycerol, the electronic and atomic contributions were neglected because they are small by comparison.[14]

The polarizability obtained here is therefore the orientation polarizability which expresses the tendency for a molecule to align itself in an electric field. It was mentioned previously that the ionization potential of organic molecules did not vary over wide limits, and inspection of data for measured ionization potentials shows that an average energy of 10 eV can be used for glycerol. The greatest uncertainty involves an estimation of the interaction distance, r, between glycerol molecules. For the present analyses, r is taken to be the diameter of the glycerol molecule (D) calculated using:[15]

$$D = 1.33 \times 10^{-8} \left(\frac{M}{\rho}\right)^{1/3} \text{ cm} , \qquad (21)$$

where M is the molecular weight and r is the density of the liquid in g/cm^3. The results for the evaluation of E_L are particularly sensitive to the value of D (5.56Å) because of the r^6 dependency in Eq. (19).

The individual contributions of the dipole, induced dipole, and dispersion energies to the total interaction attractive energy E_L in Eq. (19) as calculated for glycerol are shown in Table II.

TABLE II

CONTRIBUTIONS (%) TO VAN DER WAAL'S ENERGY FOR GLYCEROL MOLECULES

Dipole	Induced Dipole	Dispersion
8.50	3.91	87.7

Thus, we can see that the dipole coupled forces of attraction account for about 12 percent of the intermolecular binding energy between the molecules in liquid glycerol. The total Van der Waal's energy between two glycerol molecules was calculated to be E_L = 0.2 eV. This Van der Waal's bonding energy is on the order of 10 times the intermolecular bonding energy between H_2 molecules and, in general, these attractive energies are stronger with increasing size of the molecules.[16] The energies involved in intermolecular forces between molecules can also be estimated from the heat of vaporization of glycerol. The heat of vaporization of glycerol is approximately 9.5×10^5 joules/kg. If we multiply this value of H_v by the mass of a glycerol molecule and convert to electron volts, we find the energy required to break the bonds existing between glycerol molecules is ~0.9 eV. This value appears to be high, but this is consistent with the fact that glycerol has an unusually low vapor pressure. Theintermolecular bonding energies in glycerol determined from the heat of vaporization are 4.5 times that calculated by Van der Waal's energies. The discrepancy can be explained in part by the choice for the interaction distance in Eq. (19), which depends on the assumed diameter of the molecule. A drecrease in r of about 20 to 25 percent in the Van der Waal's equation will increase the binding energy a factor of four, in closer agreement with the heat of vaporization. Perhaps even more important, Eq. (19) is based upon the binding energy of two molecules rather than the multimolecular forces that exist in a solid or liquid. Thus, the number of bonds might be increased m nyfold to account for this, thereby resulting in a much larger value of E_L. In view of the uncertainty in the calculation, we shall use the value of E_L = 0.9 eV for the total cohesive energy of the charged droplet.

The total energy, E_t, of the molecular droplet system for a 50Å droplet at 20°C was calculated using Eq. (18). The relative contribution for each energy terms is shown below:

$$N_t E_L = 3700 \text{ eV}$$

$$\gamma A = 124 \text{ eV}$$

$$\frac{(Ze)^2}{4\pi \epsilon_o R} = 502 \text{ eV}$$

In the calculation, N_t was taken as the sum of the glycerol and sodium iodide molecules in the droplet, assuming that the intermolecular attractive forces acting between two glycerol molecules is essentially the same as the forces acting between a NaI molecule and a glycerol molecule. Therefore, the total energy of the droplet is $E_t \cong 3000$ eV. In the section on particle collisions, the droplet binding energy plays a key role in the examination of probable mechanisms for negative ion formation.

SECTION 4

COLLISION PROCESSES IN THE ACCELERATION REGION

4.1 SPECTROMETRIC EVIDENCE FOR COLLISIONS IN EXHAUST BEAM

4.1.1 FRAGMENT IONS

Evidence for collisions in the colloid thruster beam can be inferred from a comparison of the data available from the electron impact spectra (EI) for glycerol and the electrohydrodynamic spectra (EH) using a NaI-glycerol working fluid. EI spectra are typically generated by introducing vaporized sample molecules into an ion source chamber which are bombarded by a beam of low energy electrons. Ions produced from the collisions are focused into a mass spectrometer. Mass spectra indicating the relative amounts and masses of positive ion fragments formed by electron bombardment of glycerol molecules have been measured.[17] EH spectra are measured by the direct coupling of an electrohydrodynamic source of charged particles (e.g., colloid needle emitter) to a mass spectrometer for the detection of ionic species. This technique was recently used to study the fragment ions produced when NaI-glycerol is subjected to intense fields at a needle emitter.[18] Table III lists some glycerol fragment ions observed in common by both EH and EI spectra analyses.

Other fragment ions were observed, but those listed in Table III were easily identifiable and represent those species having the largest relative intensities for both spectra techniques.

TABLE III

FRAGMENT IONS COMMON TO EH AND EI SPECTRA FOR GLYCEROL (M < 92)

Mass	Ionic Species
31	CH_2OH^+
44	CH_2CHOH^+
61	$CH_2OHCHOH^+$

Fragment ions with mass units less than 92 measured by EH spectra are most probably the result of the bombardment of neutral glycerol molecules. This assumption appears plausible, since the major glycerol fragment ions exhibiting the highest relative intensities show up in both EH and EI spectra. The fragment ions produced in the EI measurements are clearly formed by collisions of low energy electrons with glycerol vapor. The bombarding particle hypothesized for the EH process which interacts with neutral glycerol vapor to produce fragment ions could be electrons produced in the accelerating region. These fragment ions could also be produced by collisions of energetic, positively charged molecular ions with neutral glycerol molecules. The probability of producing fragment ions ($m < 92$) from collision between charged droplets and neutral or molecular ions is assumed smaller than bombardment of neutral molecules.

In summary, evidence that fragment ions are produced in collisions and not field generated from emission sites is inferred from the similarities of fragments observed in the EH and EI collision spectra. Supporting evidence is presented in the next subsection, where field strengths necessary to generate various ionic species by EH methods are examined.

4.1.2 FIELD STRENGTHS FOR EVAPORATION OF IONS IN EHD PROCESS

In the absence of an electric field, the energy required to evaporate an ion is given by

$$Q_o = H_v + I - \emptyset \,, \tag{22}$$

where H_v is the vaporizing energy, I is the ionization energy, and $\emptyset$ is the work function or the energy gained when an electron is returned to the material. The relation between the applied electric field strength and the energy required for field evaporation of singly charged ions is expressed by the equation:[19]

$$Q = Q_o - (e^3 E_v)^{1/2} \,, \tag{23}$$

where the units are e.s.u. and e is the electronic charge and the right-hand terms shows the reduction in the total energy (Q) by the electric field required for the ions to escape. The applied accelerating field, E_v, must overcome the Schottky mirror image force acting on the molecular ion as it escapes from the liquid substance. The ion escapes when the energy barrier, Q, is reduced to zero or is very small compared with other terms in Eq. (23) so that

$$E_v = \frac{1}{e^3} (H_v + I - \emptyset)^2 . \tag{24}$$

Polarization terms are neglected in Eq. (24) as they are assumed to be very small. If the values of H_v, I, and $\emptyset$ are expressed in electron volts, Eq. (24), the evaporation fields in volts per centimeter can be calculated from:

$$E_v = 6.95 \times 10^6 (H_v + I - \emptyset)^2 \ (V/cm) \,. \tag{25}$$

Depending on the value of the applied field, E_v, molecular ions may be evaporated in various forms.

In the EHD spraying process, ions of the form $G_n \cdot Na^+$ (n is an integer), G^+, and molecular fragment ions (e.g., CH_2OH^+) denoted by G_f^+, have been detected by means of time-of-flight or EH spectra techniques (subsection 3.2). If Q_o is expressed by the appropriate physical quantities for ion formation, the evaporation fields for the ionic types listed above can be estimated. The following forms for Q_o are suggested:

$G_n \cdot Na^+$	$Q_1 = H_v$	Type I	
G^+	$Q_2 = H_v + I - \emptyset$	Type II	(26)
G_f^+	$Q_3 = E_B + I_f - \emptyset$	Type e	

where E_B is binding energy between atoms, and I_f is the ionization potential for a fragment ion. For Type I ions, the term $(I - \emptyset)$ has been dropped, since the accelerating field does not have to provide the energy for ionization. The Na^+ ion has been made available previously via the electrochemical solvation process. Thus, the energy provided in this case to evaporate Type I ions must be sufficient to overcome only the cohesive or Van der Waal forces which are represented by the vaporization energy. The production of a Type II ion under the action of intense fields is most similar to Muller's field evaporation of metallic ions. Energy is required not only for the breaking of cohesive bonds arising from extramolecular forces but must also be sufficient to ionize the glycerol molecule. Type III ions or fragment ions differ from Type II ions, since energy must be supplied to fragment the molecule by overcoming intermolecular forces. Intermolecular bonding in the glycerol molecule is covalent in nature and the bond dissociation energy for C-C is on the order of 5 to 6 eV. This is 10 to 50 times strongerthan dispersive forces connecting molecules to each other. Therefore, the evaporation energy, H_v, for Types I and II ions is replaced by E_B, the bond dissociation energy, in the activation energy expression. The ionization energy for the glycerol molecule is replaced by I_f, the ionization energy for the fragment ion. I_f will

probably be somewhat larger than I, but not significantly and will not exceed the ionization energy for the oxygen atom (13.6 eV).

The electric field strengths to generate the various ions were computed using Eq. (25) after substitution of the appropriate Q_o term previously discussed and are listed in table IV along with their likely origins.

TABLE IV

FIELD STRENGTHS REQUIRED TO EVAPORATE VARIOUS IONS BY EHD EMISSION

Type		H_v(eV)	I, I_f(eV)	E_B(eV)	E_v(V/cm)	Origin
$G_n \cdot Na^+$	(I)	0.9	--	--	$\sim 10^6$	EHD Generated
G^+	(II)	0.9	10	--	$\sim 10^8$	Collision Product
G_f^+	(III)	--	10	5	$\sim 10^9$	Collision Product

For metallic systems, ϕ represents the absolute work function that would be the energy gained by a metal in the production of ions of Type II. For the condition of Type II and Type III ion production in glycerol by EHD emission, energy should also be gained by the capture of an electron into the material following ionization. A value of 10 eV was estimated for the ionization energy of glycerol for the above calculations. An examination of tables containing ionization potentials for organic molecules indicates that a value of 10 eV is typical for organic molecules over a wide range of structural complexity.[20]

The electric field strengths existing at the tip of the emitters used in the TRW thruster are probably on the order of 10^5 V/cm. In order to produce ions of the type G_nNa^+ requires field strengths an order of magnitude greater than the fields at the emitter. Local field strengths of these magnitudes can easily be achieved in the vicinity of emission sites due to liquid spikes. In view of the extreme field strengths

(10^2 to 10^3 higher over that for the production of $G_n \cdot Na^+$ ions) required to generate G^+ or glycerol fragment ions, it is assumed that these ions are not generated by the EHD emission process. The conclusion is that ions of Types II and III observed in EH spectra are the result of collisions within the beam. It was previously mentioned that glycerol fragment ions were observed in EH spectra, but G^+ ions have also been observed.[18]

The following system of reactions is identified as collision processes in the colloid thruster exhaust beam that deserve attention:

a. Collisions between molecular ions and charged droplets
b. Collisions between molecular ions and neutral glycerol molecules
c. Collisions between molecular ions and electrons
d. Collisions between charged droplets and electrons
e. Collisions between neutral glycerol molecules and electrons
f. Charged droplet collisions with charged droplets

Collision rates and energies involved in process (a) appear more favorable as a source of negative ion formation. The other processes have been examined and found less likely as a source for negative ions for the following reasons. Process (b), collisions between molecular ions and glycerol molecules, has a low probability of occurring because of the low molecular density only a few emitter radii away from the emitter surface. In addition, neither of the species contains the iodine needed to produce the negative ion. Process (c), collisions between molecular ions and electrons, suffers from the same conditions of process (b). Process (d), collision between charged droplets and electrons, will be discussed in the next section. Process (e), collisions between molecules and electrons, also lacks the source of negative ions. Process (f), collisions between charged droplets, could possibly produce negative ions, depending upon the collision energy. This process involves a

a range of relative energies related to the range of droplet charge-to-mass ratios, but this is encompassed by process (a), where molecular ions have the highest charge-to-mass ratios in the distribution and the rest of the distribution is represented by a single particle. When the entire distribution is taken into account, the results are found not to differ greatly from the mean droplet model. Collision between droplets can occur and can produce negative ions according to the analyses discussed in the following sections. This will simply add to the results found and does not invalidate the model.

The background development of droplet energetics discussed in subsection 3.4 aids in understanding charged droplet breakup or evaporation when energy is dumped into a droplet via a collision with a molecular ion. This section will treat aspects of collisions involving droplets, since droplet breakup suggests several possible mechanisms for the production of negative ions. An analysis of electron collisions with droplets was undertaken on the assumption that some electrons reach the accelerating region either from the chamber, from thruster electrodes, or that they are formed within the region through beam collisions.

A discussion of electron collisions is given in the next subsection, followed by an analysis of molecular ion collisions with charged droplets.

4.2 ELECTRON COLLISIONS WITH CHARGED DROPLETS

An empirical relationship relating the range of monoenergetic electrons in materials as a function of energy is given by the expression:[21]

$$R = aE_o^n \ (mg/cm^2) \ , \tag{27}$$

where a and n are empirical constants and E_o is the energy of the electrons in MeV. The constants have the following values for the energy indicated:

$$a = 710, \quad n = 1.72 \quad (0.001 < E_o < 0.3 \text{ MeV})$$

The range in Eq. (27) is in units of mass per unit area, and conversion to penetration distance in units of centimeters is accomplished through the relationship $R = \rho x$ to yield:

$$x = \frac{a}{\rho} E_o^{\,n} \text{ (cm)} \tag{28}$$

where ρ is the density of the absorbing material. For glycerol, the penetration distance for electrons as a function of energy becomes:

$$x = 0.563\ E_o^{\,1.72} . \tag{29}$$

Figure 10 is a plot of the penetration (x) in glycerol as a function of electron energy in kV.

For comparison purposes, the electron range equivalent to the diameter of 50Å radius ($D = 10^{-6}$ cm) droplet is shown on the plot and occurs for an electron energy of 450 to 500 eV. Therefore, electrons colliding with a 50Å droplet with energies greater than 0.5 kV, will pass through the droplet. For example, a 1 kV electron would penetrate glycerol a distance of 4×10^{-6} cm, which is four droplet diameters. For energies less than 0.5 kV, electrons may be captured by the droplet, depending upon the angle of incidence of the collision. For electrons that originate in the chamber downstream from the thruster and reach the accelerating region, capture would take place only in the outer fringes of the accelerating region.

The energy loss per unit path length due to ionization for electrons moving through a glycerol droplet can be estimated by:[22]

$$\left(\frac{dT}{ds}\right)_{ion} = \frac{4\pi e_2^4}{m_o v} NZ_{eff} \ln\left(\frac{m_o v^2}{I_m\sqrt{2}}\right) \text{ ergs/cm}, \tag{30}$$

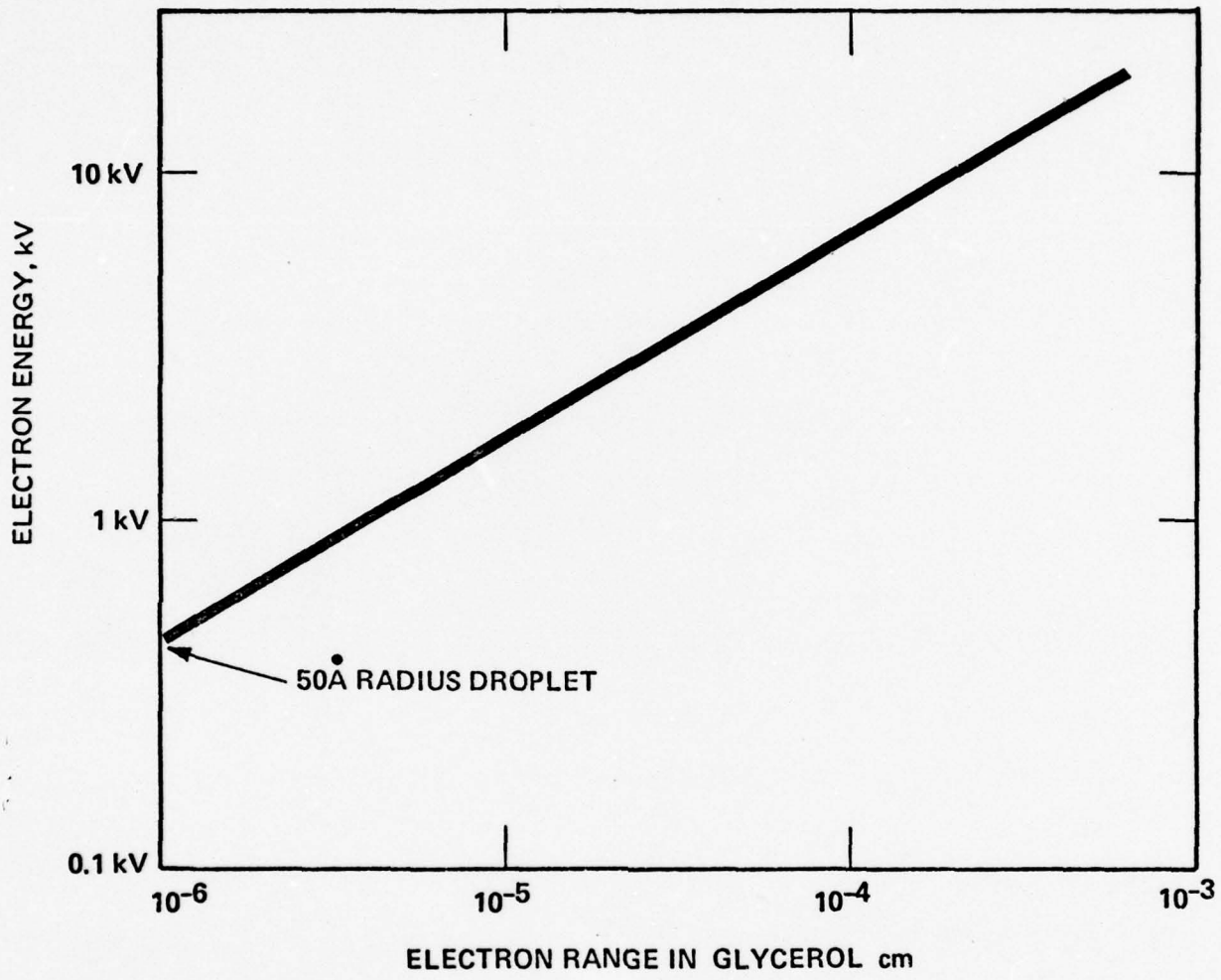

Figure 10. Range of Energetic Electrons in Glycerol

where

e = electronic charge

m_o = mass of electron

v = electron velocity

N = number of atoms/cm^3

Z_{eff} = effective value of atomic number

I_m = geometric mean ionization and excitation potential

The rate of energy loss was calculated for the special case where the electron traverses the diameter of a mean droplet. The results are shown in Figure 11, using the following values for glycerol:

N = 1.15×10^{23} atoms/cm^3

Z_{eff} = 6.16

I_m = 70.7 eV

In Eq. (30), I_m is defined as the geometric mean of the ionization and excitation potentials of the material. The I_m value for glycerol has been determined experimentally as 70.7 eV.[23] The effective value for the atomic number of glycerol was calculated on the basis that glycerol is a medium which is a mixture of N_1, N_2, and N_3 atoms/cm^3 of carbon, hydrogen, and oxygen having atomic numbers Z_1, Z_2, and Z_3, respectively. As seen in Figure 11, the maximum energy deposited in a droplet of 50Å radius is approximately 470 eV, corresponding to the electron energy just needed to escape the droplet. This energy represents one-sixth of the total droplet binding energy and could be quite effective in fragmenting the droplet. Note from Figure 11 that the energy deposited in the droplet by electrons increases linearly with the electron energy in the region for total caputre of the electron by the droplet. After the electron has enough energy to pass completely through a droplet, the amount of energy deposited decreases with increasing electron energy. High energy electrons will not deposit sufficient energy to produce

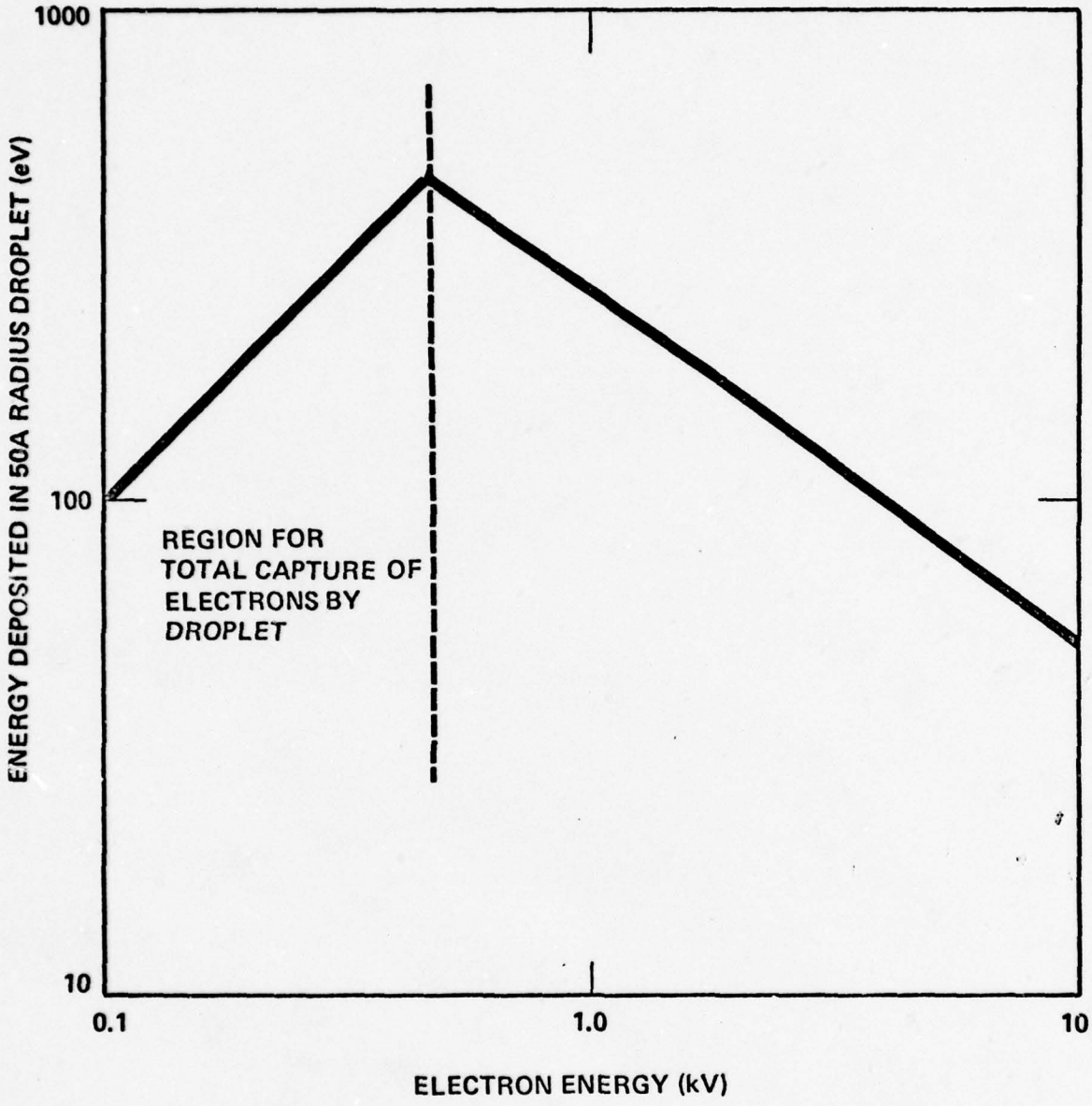

Figure 11. Energy Loss in Glycerine as a Function of Electron Energy

many ionization events within the droplet. Except for ionization at the surface, secondary electrons produced in the interior of the droplet probably lack sufficient energy to escape from the charged droplet. The secondary electrons produced by ionization in a droplet that do not escape will finally dissipate their energy in the form of heat. Collisions between electrons and droplets can result in the production of negative ions similar to the model discussed in the next section. But the number of electrons in the acceleration region is very small compared with the other species because any significant electron current will result in excessive emitter tip heating due to electron bombardment. Electron trap electrodes have been used in order to avoid this latter problem. Therefore, no significant negative ion production is expected by electron bombardment of charged droplets.

4.3 MOLECULAR ION COLLISIONS WITH CHARGED DROPLETS

The development of a collision model that satisfactorily predicts the production of negative ions of the order 10^8 to 10^9/sec will require an examination of the meaningful collision processes in the beam. The charged droplet is a carrier of iodine ions and iodine atoms, which have a large electron affinity (3.06 eV). This, coupled with the instability of the droplet for collisional energies exceeding several hundred eV, leads to the selection of the interaction between charged droplets and molecular ions as the most critical collision process for study. It is convenient to examine the collision between ion and charged droplets in terms of the collision rate given by:

$$I_c = I_o \rho \sigma x \text{ (collision/sec)} , \qquad (31)$$

where I_o is the molecular ion current (ions/sec), ρ is the density of charged droplets (#/cm^3), σ is the collision cross section (cm^2), and x is the interaction distance (cm). The cross section for this collision

is taken as the geometric cross section of the droplet which, in general, will be a function of the number of molecules in a droplet and is characterized by the symbol σ_g. The justification for using the geometric cross section was based on an analysis of charged particle scattering.

Consider the case for a positively charged ion approaching a positively charged droplet. It will experience a coulomb repulsive force referred to as Rutherford scattering. This could deflect the ion sufficiently to prevent a direct collision under certain conditions. In effect, it would decrease the collision cross section below the geometric cross section (πR^2, where R is the droplet radius).

Calculations were made using Rutherford scattering theory to determine the energy at which ions are sufficiently deflected to avoid a direct collision with the mean specific charge droplet. At high enough energies, ions collide with the droplet as long as the impact parameter is equal to R or less. Analysis shows that the assumption for the geometric cross section is valid for ion energies down to approximately 100 eV. The collision cross section drops to one-half the geometric value near 20 eV. Since most of the critical collisions will occur at energies well above 100 eV, it is sufficient to use the geometric cross section for collisions between ions and droplets.

As the charged droplet density is not constant in the accelerating region, the droplet density function $\rho(x)$ derived in subsection 3.3 will be used in the expression for collision rates. Thus,

$$I_c = I_o \sigma_g \int_{x_1}^{x_2} \rho(x)dx, \tag{32}$$

which becomes, after substitution of the density function Eq. (12),

$$I_c = I_o \sigma_g \phi \int_{x_1}^{x_2} \frac{dx}{[2C\,[V_o - V(x)]]^{\frac{1}{2}}} \quad . \tag{33}$$

This expression, therefore, describes the total number of collisions that occur over the interaction distance $x_2 - x_1$. Since the integrand of Eq. (33) contains V(x), the limits of integration can be converted from distance to potential. In terms of collision energetics, it is useful to know the total number of collisions that occur per unit time after the ion has been accelerated through a given potential difference. This was accomplished by solving the potential function for x in Eq. (1) of Section 2. With the appropriate substitutions, the expression for the collision rate can be reduced to:

$$I_c = K \int e^{y^2} dy, \tag{34}$$

where K is a constant and the integral, known as Dawson's integral, is tabulated in handbooks.[24] The constant K is given by:

$$K = r_o I_o \sigma_g \phi \left[\frac{\ln\left(\frac{2R}{r_o}\right)}{2\,C\,V_o}\right]^{\frac{1}{2}} \tag{35}$$

Collision rates were calculated for the following set of conditions:

$V_o = 13$ kV

$C = 10^4$ C/kg

$R = 1.57 \times 10^{-3}$

$r_o = 7.8 \times 10^{-4}$

$I_o = 6 \times 10^{12}$ ions/sec

$\phi = 2.04 \times 10^{19}$ droplets/m^2-sec

$\sigma_g = 7.85 \times 10^{-1^-}$ m^2

The results are shown in Figure 12, where the total number of molecular ion/droplet collisions, I_c, which occur after the ion has been accelerated through a given potential is plotted as a function of that potential. For example, molecular ions that have been accelerated from the emitter through a potential of 3 kV will then undergo 7.6×10^8 collisions with droplets before leaving the accelerating region. Note that for high energy collisions involving molecular ions that have been accelerated through at least 10 kV, the collision rates are still on the order of 10^8/second. The collisional energy for the molecular ion/droplet system is approximated by

$$E_c = 1/2\ \mu\ v_{ion}^2, \qquad v_{ion} \gg v_D, \tag{36}$$

where μ is the reduced mass and v_{ion}, the velocity of the molecular ion, is much greater than the droplet velocity v_D. Further, since the droplet mass is much greater than the mass of the molecular ion, M_{ion}, Eq. (36) becomes:

$$E_c = 1/2\ M_{ion}\ v_{ion}^2 = qV.$$

Thus, the collisional energy in electron volts involving singly charged ions and heavy charged droplets can be estimated by the potential through which the ion has been accelerated at the time of the collision. Collisions between droplets and ions that have been accelerated through 10 kV involve collision energies three times greather than the droplet total binding energy ($E_c \sim 3E_t$). From Figure 12, the number of collisions at energies of E_t or greater is larger than 10^8. Assumed production rates of 1 negative ion per collision would then erode about 1 mil/year at sputtering yields even as low as 1 atom/ion.

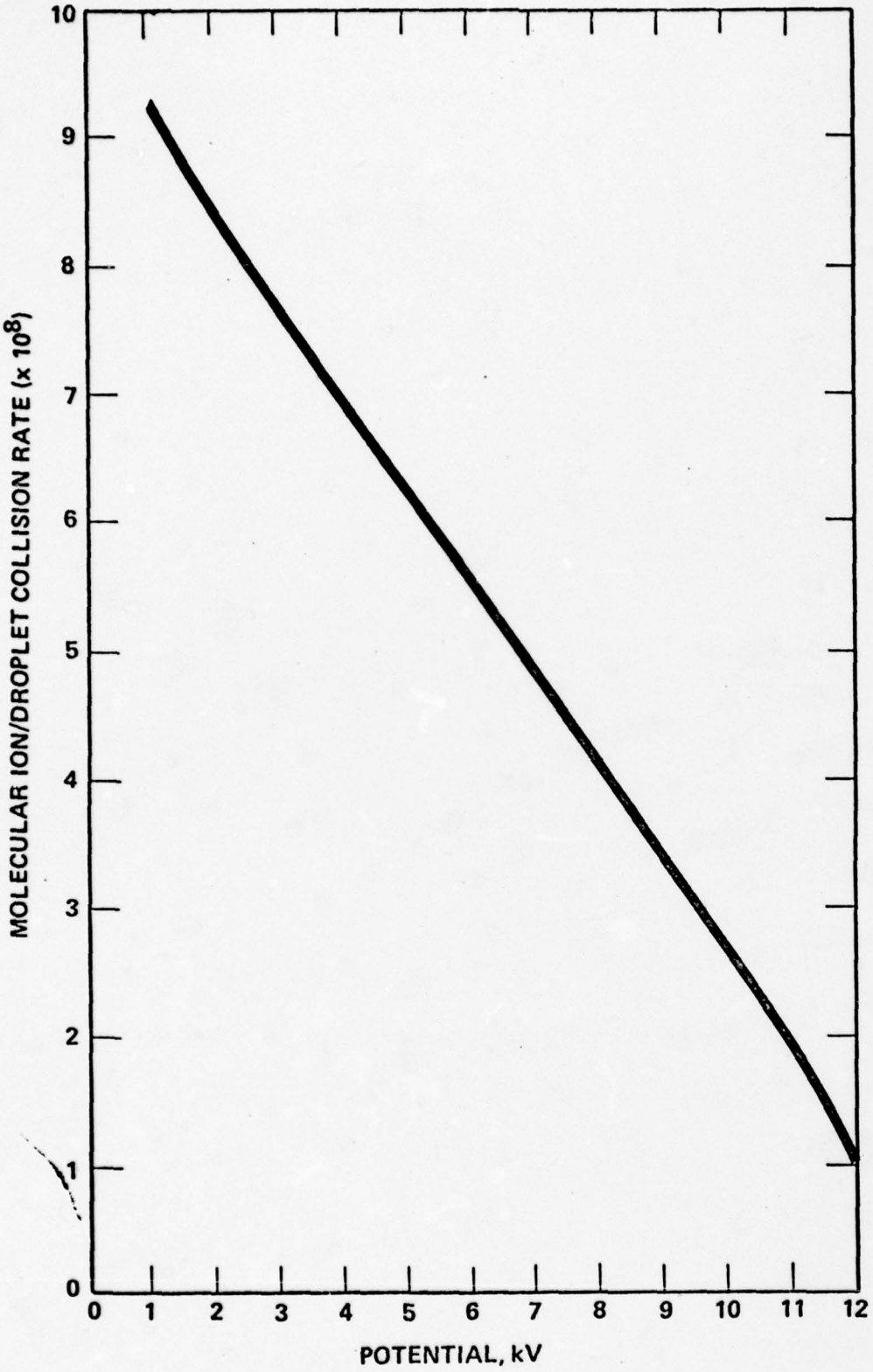

Figure 12. Total Number of Molecular Ion-Droplet Collisions Occurring after Ion Has Been Accelerated Through Potential Shown on Abscissa

4.4 EVAPORATION FROM CHARGED DROPLETS

The charged liquid droplets generated and accelerated through the intense electric field at the emitter can undergo various interactions with the fields and other particles. Each of these interactions affects the stability of the droplets and may lead to particle breakup. Particle breakup could also occur due to the inherent instabilities initiated by conditions other than collisions and interactions.

When charged droplets are generated, they are assumed limited by the Rayleigh criterion. That is, the droplet size and total charge are limited so that the maximum charge-to-mass ratio for glycerine is given by:

$$C = 3.54 \times 10^{-9} r^{-3/2} , \qquad (37)$$

where C is in units of coulombs per kilogram and r is the droplet radius in meters. Droplets can be generated with charge-to-mass ratios equal to or less than the value of C in Eq. (37). However, since the droplets undergo oscillations upon generation, they will show some instability because the Rayleigh criterion is based upon the droplets being spherical. Thus, the tendency toward droplet breakup will, in part, depend upon the oscillatory behavior. The oscillation frequency is related to viscosity which, in turn, depends strong upon temperature. Unfortunately, little is presently known about microscopic droplet oscillations and the effects of oscillations upon stability during the generation and acceleration processes. Similarly, little is known about the droplet temperature upon generation. It is suspected that the temperature is far greater than the emitter tip temperature (typically at $25^{o}C$) as a result of the current flow during the generation process.

Neutral molecule evaporation from the charged droplet will occur at a rate dependent upon the temperature. This evaporation could cause a

rapid decrease in the droplet size so that the radius decreases and the charge-to-mass ratio increases, resulting in a departure from the limiations of the Rayleigh criterion as expressed by Eq. (37). This phenomenon was described by Abbas and Latham[25] in which evaporation and successive droplet instabilities were observed.

As discussed previously, the droplet temperature can undergo a drastic increase as a result of a collision with an energetic ion. This could cause partial or even total evaporation. If the evaporation time is comparable to the time spent in the accelration region, the probability of generating negative ions which can return to the emitter is greatly enhanced. The time required for heat to transfer throughout the droplet from a collision would be about 10^{-11} seconds, assuming that heat transfer propagates at the velocity of sound for such a small droplet. This is a short time comparted to the acceleration region transit time ($\sim 10^{-7}$ sec). It would be of interest to compare the evaporation time for various temperatures with the above transit time.

The time for the droplet to evaporate 90 percent of ots mass was calculated and defined as the evaporation time (τ). This time decreases with increasing temperature in accordance with the evaporation rate. The calculation was simplified, since it is for comparative purposes, and some factors were neglected. The temperature is lowered by evaporation which increases the evaporation time. The evaporation rate goes up as the droplet size decreases, which decreases the evaporation time. These two important parameters will be discussed later and their effect upon the calculations considered.

The change per unit time in the number of molecules (n) in the droplet due to evaporation is given by

$$\frac{dn}{dt} = -J_T A(t) , \qquad (38)$$

where J_T is the molecular evaporation rate in molecules/m^2-sec, and A(t) is the droplet area which varies with time. Assume the droplet radius is R = 50Å, and the volume of a molecule in the droplet is $V = (5Å)^3$, Eq. (38) becomes

$$\frac{dn}{n^{2/3}} = J_T(36\pi)^{1/3} V^{2/3} dt . \tag{39}$$

This equation is integrated from n_o, the initial number of molecules, to 0.1 n_o on the left, and from 0 to τ on the right. After integration, the evaporation time is found to be

$$\tau = \frac{3(0.464)\ n_o^{1/3}}{J_T(36\pi)^{1/3} V^{2/3}} . \tag{40}$$

Considering droplets raised to various temperatures at generation, due to collisions or for any other condition, the evaporation times and the evaporation rates are given in Table V.

TABLE V

EVAPORATION TIME

Temperature °celcius	Evaporation Rate J_T(mol/m^2-sec)	Evaporation Time τ (sec)
20	10^{20}	2.09×10^{-1}
50	1.8×10^{21}	1.16×10^{-2}
100	1.4×10^{23}	1.49×10^{-4}
150	3.09×10^{24}	6.8×10^{-6}
200	2.7×10^{25}	7.7×10^{-7}
290	4.46×10^{26}	4.68×10^{-8}

From the results given in Table V, illustrated in Figure 13, droplets with temperatures well above 200°C will undergo total evaporation within the acceleration region. But partial evaporation is possible, resulting in Rayleigh instabilities down to temperatures close to 100°C, since approximately 30 percent of the droplet will evaporate in one-fifth of the calculated evaporation time. In theory, collisions with ions having energies of a couple of kV or more will undoubtedly result in droplet disintegration within the acceleration region. Below these energies, droplet fragmentation will readily occur with perhaps less probability of negative ion production.

Since the decrease in temperature due to evaporation was not included, the evaporation times would be increased above the calculated values. To include cooling effects, the heat of vaporization, the specific heat, and the thermal evaporation rate must be carried as variables, and these functions do not have simple analytic expressions. However, the increase in evaporation time is somewhat balanced by a corresponding increase in evaporation rate with decreasing droplet size.[26] This is due to the droplet curvature approaching molecular dimensions and loss of bonds holding the molecules on the surface. When the droplet radius decreases to one-fifth of its initial size, the evaporation rate increases by close to a factor of three.

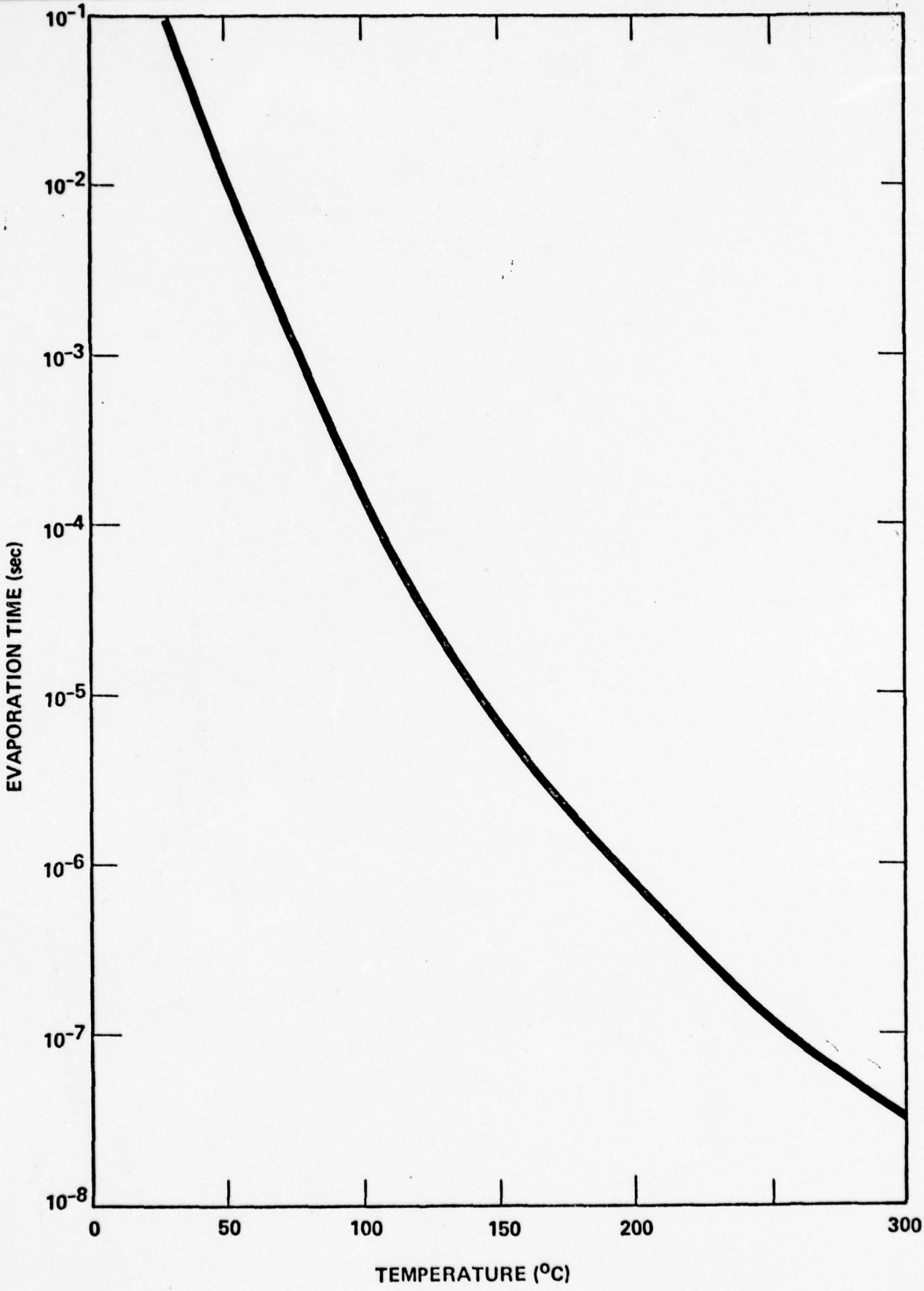

Figure 13. Evaporation Time for R = 50Å Droplet to 10 Percent of Mass

SECTION 5

EFFECT OF A DISTRIBUTION OF DROPLETS ON THE COLLISION RATE

The charged glycerine particles emitted from the EHD source can be classified into two separate groups. The first group, which constitutes approximately 91 percent of the total number of charged particles, consists of charged liquid droplets. The second group consists of singly charged molecular ions. In the first group, the mean value of the charge-to-mass ratio (q/m) is, $\overline{q/m} = 10^4$ C/kg, and in the second group it is, $\overline{q/m} = 4.62 \times 10^5$ C/kg. Since both groups are accelerated by the same electrical potential, the velocity of the ions will be approximately seven times greater than that of the droplets. The faster moving ions constitute an electric current which passes through the aggregate of slower moving droplets. It is of interest to determine the collision rate of the ions as a function of the distance traversed by them through the relatively motionless droplets.

5.1 DEFINITION OF ION COLLISION RATE

Let I_o denote the initial magnitude of the molecular ion current, and let I denote the current after it has moved a distance, x, through the "fixed" group of droplets. Now, the number of singly charged molecular ions leaving the ion source in time, Δt, is, $(I_o/e)\Delta t$, where, e = charge on electron = 1.6×10^{19} coulombs. The number of singly charged molecular ions that survive a distance x (do not make collisions) through the droplets in time Δt is, $(I/e)\Delta t$. The number of ions that collide with the droplets is then, $(I_o/e)\Delta t - (I/e)\Delta t$ and the collision rate, β, is this quantity divided by Δt. Thus,

$$\beta(x) = \frac{I_o - I(x)}{e}, \text{ collisions/sec.} \qquad (41)$$

To determine $\beta(x)$, an expression for $I(x)$ must first be derived. This is done in the following paragraphs.

5.2 MOLECULAR ION CURRENT

5.2.1 DROPLET VELOCITY

It is assumed that the liquid droplets are spherical and that their radii are generally unequal. Let $\sigma(r_i)$ denote the collision cross section of those droplets that have a radius r_i, and let $n(r_i)$ denote the particle number density of these same droplets. Then, the reduction in the ion current, dI, after traversing a distance, dx, is given by

$$dI = -I\left[\sum_i \sigma(r_i)n(r_i)\right]dx \ , \tag{42}$$

where the quantity, $\sum_i \sigma(r_i)n(r_i)$, represents the "absorption coefficient" of the ions. Here,

$$\sigma(r) = \pi r^2 \ , \tag{43}$$

$$n(r) = \frac{\dot{N}_r}{Av_r} \ , \tag{44}$$

where A = total cross-sectional area of the ion beam, v_r = velocity of those droplets having a radius r, and $\dot{N}_r$ = flow rate (particles/sec) of those droplets having a radius r.

The molecular ions and charged liquid droplets are both accelerated through a potential difference, $V_o - V(x)$, where V_o = potential at the charged particle emitter, and $V(x)$ = potential at a distance x from the emitter along the axis of symmetry. A good approximation of this potential taken from Section 3 is given by

$$V(x) = V_o \frac{\ell n\left(\frac{a}{x+b}\right)}{\ell n\,(a/b)} , \quad (x \leq a) , \tag{45}$$

where, $a = 1.57 \times 10^{-3}$ meters, $b = 3.9 \times 10^{-4}$ meters, and, $V_o = 13{,}000$ volts. Note that, $V(0) = V_o$. The velocity acquired by those droplets having a charge-to-mass ratio, q/m, after being accelerated through a distance x is

$$v = \sqrt{2}\left[V_o - V(x)\right]^{1/2} (q/m)^{1/2} . \tag{46}$$

It is experimentally verifiable that q/m is related to the droplet radius, r, fairly accurately, by

$$\frac{q}{m} = \frac{3(\epsilon_o \gamma)^{1/2}}{\rho r^{3/2}} , \tag{47}$$

where, ϵ_o = permittivity of free space = 8.854×10^{-12} farads/meter, γ = surface tension of droplet = 1.3 newtons/meter, ρ = density of droplet = 8000 kg/meter^3. Combining Eqs. (46) and (47) yields the desired droplet velocity.

$$v_r = \sqrt{2}\left(\frac{9\epsilon_o \gamma}{2}\right)^{1/4} \left[V_o - V(x)\right] \frac{1}{r^{3/4}} . \tag{48}$$

Since $v_r = 0$ when $x = 0$, therefore, from Eq. (44) the particle number density becomes infinite at $x = 0$. Since this is not a realistic result, the minimum allowable value of x, denoted by x_o, must be made greater than zero. A practical value of x_o is assumed to be that which satisfies the equation,

$$V_o - V(x_o) = 100 \text{ volts} , \tag{49}$$

since the faster moving ions only begin to break up the droplets into separate ions (by collision) after the molecular ions have been accelerated through a potential difference of approximately 100 volts. Substituting Eq. (45) into Eq. (49) yields

$$x_o = 4.23 \times 10^{-6} \text{ meters.}$$

5.2.2 DROPLET FLOW RATE

Experimental results suggest that the charge-to-mass ratio, q/m, of the droplets is normally distributed. Thus, if f(q/m) denotes the probability density function of q/m, then

$$f(q/m) = \frac{1}{S(2\pi)^{1/2}} \exp\left[-\frac{1}{2}\left(\frac{q/m - \overline{q/m}}{S}\right)^2\right] \tag{50}$$

where, S and $\overline{q/m}$ are the standard deviation and mean, respectively, of the distribution. As stated earlier, $\overline{q/m} = 10^4$ C/kg. Also, S $\approx$ 3000 C/kg. Since the droplet radius, r, is related to q/m through Eq. (47), therefore, the probability density function of r, denoted by g(r), can also be obtained. It is given by

$$g(r) = f(q/m)\left|\frac{d(q/m)}{dr}\right|$$

$$= \frac{3}{2}\left(\frac{9\epsilon_o\gamma}{\rho^2}\right)^{1/2} \frac{r^{-5/2}}{S(2\pi)^{1/2}} \exp\left\{-\frac{1}{2S^2}\left[\left(\frac{9\epsilon_o\gamma}{\rho^2}\right)^{1/2} r^{-3/2} - \overline{q/m}\right]^2\right\} \tag{51}$$

Note that $g(0) = 0$. If $\dot{N}$ denotes the total flow rate of the droplets, then it follows that,

$$\dot{N}_r = \dot{N} \int_r^{r+\Delta r} g(v)\, dv = \dot{N} g(r) \Delta r , \tag{52}$$

where, Δr is an infinitesimal.

Since $\dot{N}$ represents the total flow rate of the droplets, therefore, the electric current, i, generated by the motion of the charged droplets can be expressed by

$$i = \dot{N} \bar{q}$$

where $\bar{q}$ denotes the mean charge of the droplets. Now the total current, I_T, leaving the emitter is given by

$$I_T = i + I_o$$

where I_o is the initial molecular ion current. Since i is approximately ten times the magnitude of I_o, therefore, $i = 10\, I_T/11$. Let, $I_T/A = J_T$, denote the total current density at the ion source. Hence,

$$\frac{\dot{N}}{A} = \frac{10}{11} \frac{J_T}{\bar{q}} \approx \frac{J_T}{\bar{q}} \tag{53}$$

The quantity J_T can be measured. The mean droplet charge, $\bar{q}$, is determined as follows. Since the droplets are assumed to be spherical, the droplet mass, m, is then given by, $m = 4\pi r^3 \rho/3$. By combining this equation with Eq. (47), it is easy to show that

$$q = \frac{12\, \pi \gamma \epsilon_o}{\rho} \frac{1}{q/m} . \tag{54}$$

The probability density function of q, denoted by h(q), is then given by

$$h(q) = f(q/m)\left|\frac{d(q/m)}{dq}\right| = \frac{12\pi^{\gamma}\epsilon_o}{\rho q^2} f(q/m) , \qquad (55)$$

where, f(q/m) is expressed in terms of q, via Eq. (54). By definition, the mean value of q in the interval, $q_1 \leq q \leq q_2$, is given by

$$\bar{q} = \int_{q_1}^{q_2} qh(q)dq \qquad (56)$$

where, h(q) is given by Eq. (55), and

$$q_1 = \frac{12\pi\gamma\epsilon_o}{\rho}\frac{1}{(q/m)_1} , \qquad q_2 = \frac{12\pi\gamma\epsilon_o}{\rho}\frac{1}{(q/m)_2} .$$

The values assigned to $(q/m)_1$, and $(q/m)_2$ should be chosen so that they include practically all possible values of q/m. Since q/m is normally distributed, therefore, the following assigned values of $(q/m)_1$ and $(q/m)_2$ will bracket 99.73 percent of all possible values of q/m:

$$\begin{aligned} (q/m)_1 &= \overline{q/m} + 3S = 19{,}000 \text{ coulombs/kg} \\ (q/m)_2 &= \overline{q/m} - 3S = 1{,}000 \text{ coulombs/kg} \end{aligned} \qquad (57)$$

By introducing a change of variable from Eq. (54), and making use of Eq. (55), it is easy to show that Eq. (56) becomes,

$$\bar{q} = \int_{1{,}000}^{19{,}000} \frac{12\pi\gamma\epsilon_o}{\rho}\frac{1}{q/m} f(q/m)d(q/m) , \qquad (58)$$

where, f(q/m) is given by Eq. (50).

5.2.3 MOLECULAR ION CURRENT

By combining Eqs. (53), (52), (48), (44), and (43), one obtains the following:

$$\sum_i \sigma(r_i)n(r_i) = \frac{\pi J_T}{\sqrt{2}\,\bar{q}} \left(\frac{\rho^2}{9\gamma\epsilon_o}\right)^{\frac{1}{4}} \left[V_o - V(x)\right]^{-\frac{1}{2}} \sum_i r_i^{\frac{11}{4}} g(r_i)\Delta r_i$$

$$= \frac{\pi J_T}{\sqrt{2}\,\bar{q}} \left(\frac{\rho^2}{9\gamma\epsilon_o}\right)^{\frac{1}{4}} \left[V_o - V(x)\right]^{-\frac{1}{2}} \int_{r_1}^{r_2} r^{\frac{11}{4}} g(r)dr \,, \tag{59}$$

where, $r_2 > r_1$ and

$$r_1 = \left(\frac{9\gamma\epsilon_o}{\rho^2}\right)^{1/3} \frac{1}{(q/m)_1^{2/3}}, \qquad r_2 = \left(\frac{9\gamma\epsilon_o}{\rho^2}\right)^{1/3} \frac{1}{(q/m)_2^{2/3}} .$$

By introducing a change of variable from Eq. (47) and making use of the first part of Eq. (51), it follows that:

$$\int_{r_1}^{r_2} r^{\frac{11}{4}} g(r)dr = \left(\frac{9\gamma\epsilon_o}{\rho^2}\right)^{11/12} \int_{1,000}^{19,000} (q/m)^{-11/6} f(q/m)d(q/m) \tag{60}$$

Now, integrating Eq. (42) yields

$$I(x) = I_o \exp\left[-\int_{x_o}^{x} \sum_i \sigma(r_i)n(r_i)dx\right] \tag{61}$$

Substituting Eqs. (60) and (59) into Eq. (61) finally yields the desired expression for the molecular ion current:

$$I(x) = I_o \exp\left\{-\frac{\pi J_T}{\sqrt{2}\,\bar{q}}\left(\frac{9\gamma\epsilon_o}{\rho^2}\right)^{2/3}\int_{1,000}^{19,000}(q/m)^{-11/6}\,f(q/m)\,d(q/m)\cdot\int_{x_o}^{x}\frac{dx}{[V_o - V(x)]^{\frac{1}{2}}}\right\} \tag{62}$$

where, $x_o = 4.23 \times 10^{-6}$ meters and V(x) is given by Eq. (45).

5.3 ION COLLISION RATE

Recall that the ion collision rate is given by Eq. (41), where I(x) is given by Eq. (62). A realistic value of the total ion current is, $I_T = 9.6 \times 10^{-6}$ amperes, and the cross-sectional area of the ion beam is, $A = \pi(7 \times 10^{-3}\ \text{inch})^2$. Hence,

$$J_T = \frac{I_T}{A} = 96.67\ \text{amperes/meter}^2.$$

From the values of γ, ϵ_o, and ρ given in subsection 5.2, it follows that

$$\left(\frac{9\gamma\epsilon_o}{\rho^2}\right)^{2/3} = 1.3785 \times 10^{-12}\ (\text{coulombs/kg})^{4/3}\ \text{meters}^2.$$

Next, employing the trapezoidal rule (numerical integration), the integrations needed to determine $\bar{q}$, given by Eq. (58), and the first integral in Eq. (62), yield the following:

$$\bar{q} = 6.1288 \times 10^{-18} \text{ coulombs } (= 38.3 \text{ e}) ,$$

$$\int_{1,000}^{19,000} (q/m)^{-11/6} f(q/m)d(q/m) = 6.6953 \times 10^{-8} (\text{coulombs/kg})^{-11/6}$$

Finally, the second integral in Eq. (62) can be simplified by introducing the change of variable,

$$z = \left[\frac{1}{V_o} \ell n(a/b)\right]^{\frac{1}{2}} \left[V_o - V(x)\right]^{\frac{1}{2}} = \left[\ell n(a/b) - \ell n\left(\frac{a}{x+b}\right)\right]^{\frac{1}{2}} .$$

Thus,

$$\int_{x_o}^{x} \frac{dx}{[V_o - V(x)]^{\frac{1}{2}}} = 2bk \int_{z_o}^{z(x)} e^{z^2} dz , \qquad (63)$$

where,

$$k = \left[\frac{1}{V_o} \ell n(a/b)\right]^{\frac{1}{2}} , \qquad z(x) = k\left[V_o - V(x)\right]^{\frac{1}{2}}$$

and, $z_o = z(x_o)$. The transformed integral in Eq. (63) can be expressed in terms of Dawson's integral, given by

$$F(y) = e^{-y^2} \int_o^y e^{t^2} dt . \qquad (64)$$

Values of F(y) can be found tabulated, for, $0 \leq y \leq 2.00$, in "Handbook of Mathematical Functions," National Bureau of Standards, Applied Mathematics Series 55, 1964. From Eqs. (63) and (64), one obtains

$$\int_{x_o}^{x} \frac{dx}{[V_o - V(x)]^{\frac{1}{2}}} = 2bk \left\{e^{z^2(x)} F[z(x)] - e^{z_o^2} F(z_o)\right\} \qquad (65)$$

Employing the values of a, b, V_o given in subsection 5.2, we have:

$$2\,bk = 8.0732 \times 10^{-6} \text{ (coulombs/kg)}^{\frac{1}{2}} \text{ sec} ,$$

$$z(x) = [1.39268 + \ell n(636.94\,x + 0.2484)]^{\frac{1}{2}} ,$$

$$z_o = 0.103697$$

Note that, since, $x_o \leq x \leq a$, therefore,

$$z_o \leq z(x) \leq 1.27 .$$

Hence, the tabulated values of F(y), for $0 \leq y \leq ^{\wedge}.00$, given in the above reference, will be sufficient for evaluating the integral in Eq. (65). Substituting all of the foregoing in Eq. (62) yields the desired molecular ion current:

$$I(x) = I_o \exp\left[- 2.61\ (10^{-5}) \left\{ e^{z^2(x)}\ F[z(x)] - 1.01\ F(z_o) \right\} \right] . \qquad (66)$$

The ion collision rate is then obtained by substituting Eq. (66) into Eq. (41).

Before the collision rate, β, can be calculated, the initial ion current, I_o, must be evaluated. Recall that $i = 10\ I_o$ and $i = 10\ I_T/11$, so that $I_o = I_T/11 = 9.6 \times 10^{-6}/11 = 8.727 \times 10^{-7}$ amperes. The lower solid curve in Figure 14 shows a plot of the ion collision rate versus the axial distance, x, from the tip of the emitter. Here, the collisions between the ions and the droplets occur all along the axial distance from x_o to x. Note that the total collision rate therefore occurs at $x = a$, i.e., at the end of the acceleration region and it is equal to 3.35×10^8 collisions/sec.

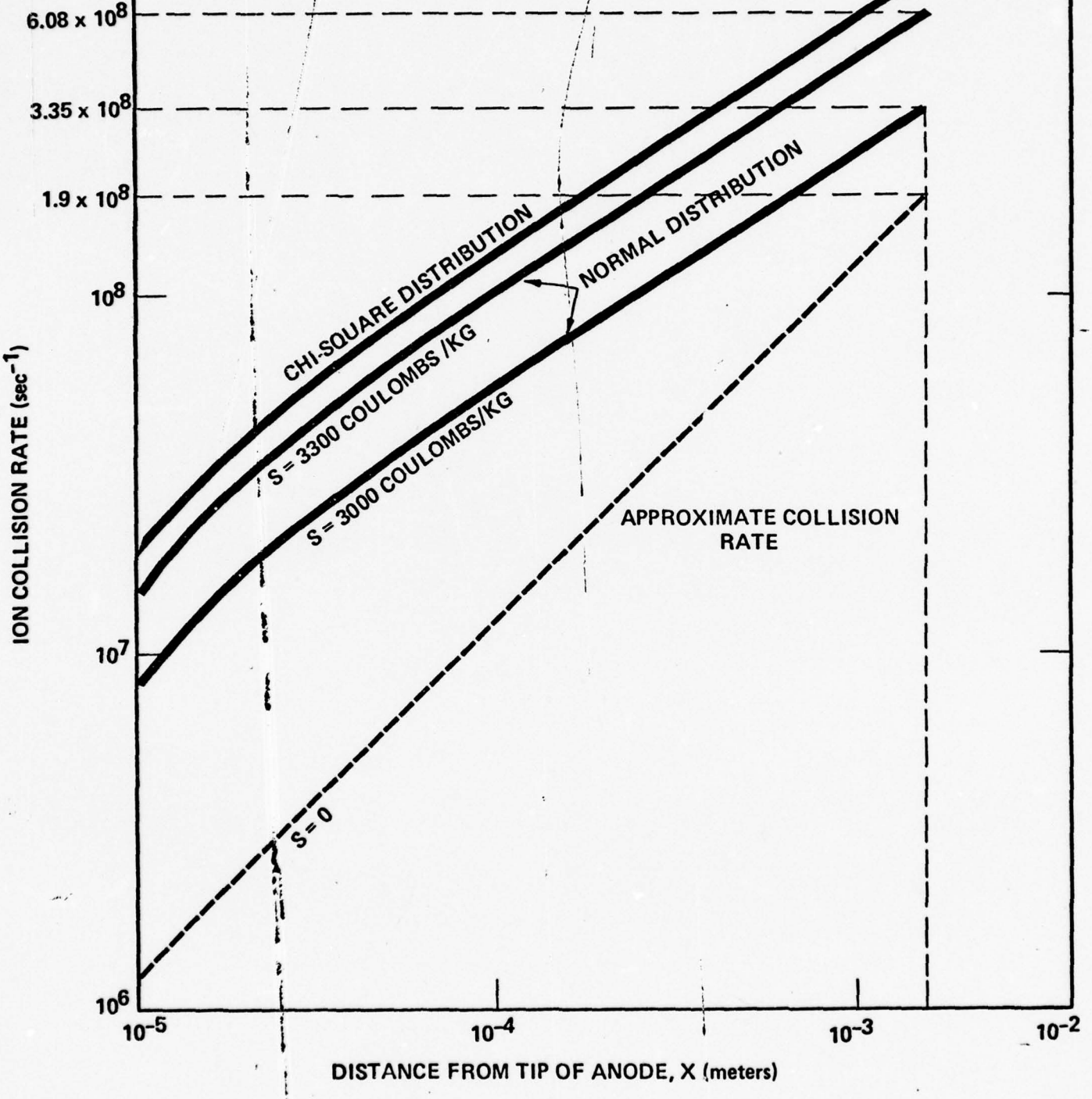

Figure 14. Molecular Ion Collision Rate versus Axial Distance from the Emitter Tip

Recall that the standard deviation of the probability density function of q/m, given by Eq. (50), is S = 3,000 coulombs/kg. What effect will an increase in S have on the ion collision rate? To answer this question, let S = 3,300 coulombs/kg. Then the upper and lower limits of integration in Eqs. (58) and (62) become 19,900 coulombs/kg and 100 coulombs/kg, respectively. Hence,

$$\overline{q} = 6.4868 \times 10^{-18} \text{ coulombs},$$

and

$$\int_{100}^{19,900} (q/m)^{-11/6} f(q/m)d(q/m) = 1.2854 \times 10^{-7} \text{ (coulombs/kg)}^{-11/6},$$

so that Eq. (62) then becomes

$$I(x) = I_o \exp\left[-4.73(10^{-5})\left\{e^{z^2(x)} F\left[z(x)\right] - 1.01\, F(z_o)\right\}\right].$$

Substituting the above in Eq. (41) yields the ion collision rate. The middle solid curve in Figure 14 shows the ion collision rate versus the distance, x. Note that when x = a, the collision rate is 81 percent greater than that for the case S = 3,000 coulombs/kg. Thus, a 10 percent increase in S causes an 81 percent increase in the collision rate at x = a.

5.4 APPROXIMATE ION COLLISION RATE

Although Eq. (66) gives an accurate description of the molecular ion current, it is worthwhile to consider an approximate representation of this current as discussed in Section 4. The approximation can be readily derived by making the following two assumptions:

a. All the droplets have the same charge-to-mass ratio, given by, $q/m = 10^4$ coulombs/kg.

b. The velocity of the droplets is independent of x, i.e., the velocity is constant.

As a consequence of (a), and by virtue of Eq. (47), all droplets will have the same radius, given by $r = 2.5295 \times 10^{-9}$ meters. As a consequence of (b), Eq. (46) becomes, $v = (2\Delta V)^{\frac{1}{2}}(q/m)^{\frac{1}{2}}$, where, $\Delta V = 13{,}000$ volts, so that, $v = 16{,}125$ meters/sec. As a further consequence of assumptions (a) and (b), both the collision cross section and the particle number density of the droplets, given by Eqs. (43) and (44), respectively, are constant. Hence, Eq. (42) becomes

$$dI = -I\sigma n dx ,$$

which readily integrates to

$$I(x) = I_o e^{-\sigma n x} . \tag{67}$$

Now, from Eq. (43), $\sigma = 2.0101 \times 10^{-17}$ meters^2. Since the droplet velocity is assumed constant, Eq. (44) becomes

$$n = \frac{\dot{N}}{Av}$$

where, from Eq. (53),

$$\frac{\dot{N}}{A} = \frac{J_T}{q} .$$

Here, q is determined from Eq. (54), so that

$$q = 5.424 \times 10^{-18} \text{ coulombs.}$$

Then, since, $J_T = 96.67$ amperes/meters^2, therefore,

$$n = \frac{J_T}{qv} = 1.1052 \times 10^{15} \text{ particles/meter}^3.$$

Substituting the above values of σ and n in Eq. (67), the approximate ion current becomes

$$I(x) = I_o e^{-0.0222x} \tag{68}$$

where, $I_o = 8.727 \times 10^{-7}$ amperes. The approximate ion collision rate is then obtained by substituting Eq. (68) into Eq. (41).

The dashed curve in Figure 14 shows the approximate ion collision rate as a function of x, where the collisions occur all along the axial distance from x = 0 to x. Note that when x = *a*, the approximate total collision rate is only 43 percent less than the collision rate for S = 3,000 *coulombs/kg*.

In view of the assumption (a) above, the probability density function for q/m can here be taken as the normal distribution with a standard deviation of $\underline{S = 0}$.

5.5 A NON-NORMAL PROBABILITY DENSITY FUNCTION

5.5.1 THE CHI-SQUARE DISTRIBUTION

The ion collision rate is critically dependent on the probability density function, f(q/m), of the charge-to-mass ratio, as evidenced by Eqs. (62) and (41). In the foregoing treatment, it was assumbed that f(q/m) was the normal (Gaussian) distribution, given by Eq. (50). It would be interesting to allow f(q/m) to assume a different form and then learn what effect this new function has on the ion collision rate. A

probability density function which resembles a skewed normal distribution is the Chi-Square Distribution, given by

$$\frac{(\chi^2)^{\frac{\nu}{2}-1} e^{-\chi^2/2}}{2^{\frac{\nu}{2}} T(\frac{\nu}{2})}, \quad (\chi^2 \leq 0)$$

where, ν = positive integer. Let z be a dimensionless variable, given by

$$z = C \frac{q}{m}$$

where, C is a positive constant. By replacing χ^2 with z in the above expression, it is easy to show that the new probability density function for q/m is given by

$$f(q/m) = \frac{C^{\frac{\nu}{2}}}{2^{\frac{\nu}{2}} T(\frac{\nu}{2})} (q/m)^{\frac{\nu}{2}-1} e^{-\frac{1}{2} C q/m} \tag{69}$$

where,

$$\int_0^{\infty} f(q/m) d(q/m) = 1$$

The mean and standard deviation of f(q/m) are given, respectively, by

$$\overline{q/m} = \frac{\nu}{C},$$

and

$$S = \frac{1}{C} (2\nu)^{\frac{1}{2}}$$

Note that $\overline{q/m}$ and S are not independent, as they are for the normal distribution. We shall let $\overline{q/m}$ = 10,000 coulombs/kg. Hence,

$$C = \frac{\nu}{10{,}000} \text{ kg/coulomb} .$$

The following value is assigned, $\nu = 4$. Therefore,

$$C = 4.0 \times 10^{-4} \text{ kg/coulomb} .$$

Hence, S = 7071 coulombs/kg. Figure 15 shows a plot of f(q/m) versus q/m, where, f(q/m) is given by Eq. (69). The dashed curve in Figure 15 is f(q/m), given by Eq. (50), where $\overline{q/m}$ = 10,000 coulombs/kg and S = 3,000 coulombs/kg.

5.5.2 ION COLLISION RATE

From Eqs. (69) and (47), the probability density function of the droplet radius, r, becomes

$$g(r) = \frac{C^{\frac{\nu}{2}}}{2^{\frac{\nu}{2}}\,\Gamma(\frac{\nu}{2})} \cdot \frac{3}{2}\left(\frac{9\gamma\epsilon_o}{\rho^2}\right)^{\frac{\nu}{4}} \frac{1}{r^{\frac{3\nu}{4}+1}} \exp\left[-\frac{C}{2}\left(\frac{9\gamma\epsilon_o}{\rho^2}\right)^{\frac{1}{2}} r^{-3/2}\right] \qquad (70)$$

From Eq. (60), we have

$$\int_{r_1}^{r_2} r^{\frac{11}{4}}\, g(r)\,dr = \left(\frac{9\gamma\epsilon_o}{\rho^2}\right)^{11/12} \int_{(q/m)_2}^{(q/m)_1} (q/m)^{-11/6}\, f(q/m)\,d(q/m) ,$$

where, f(q/m) is now given by Eq. (69), and, $(q/m)_1 > (q/m)_2$.

The values assigned to $(q/m)_1$ and $(q/m)_2$ should be chosen so that they include practically all possible values of q/m. Since z(= C q/m) obeys

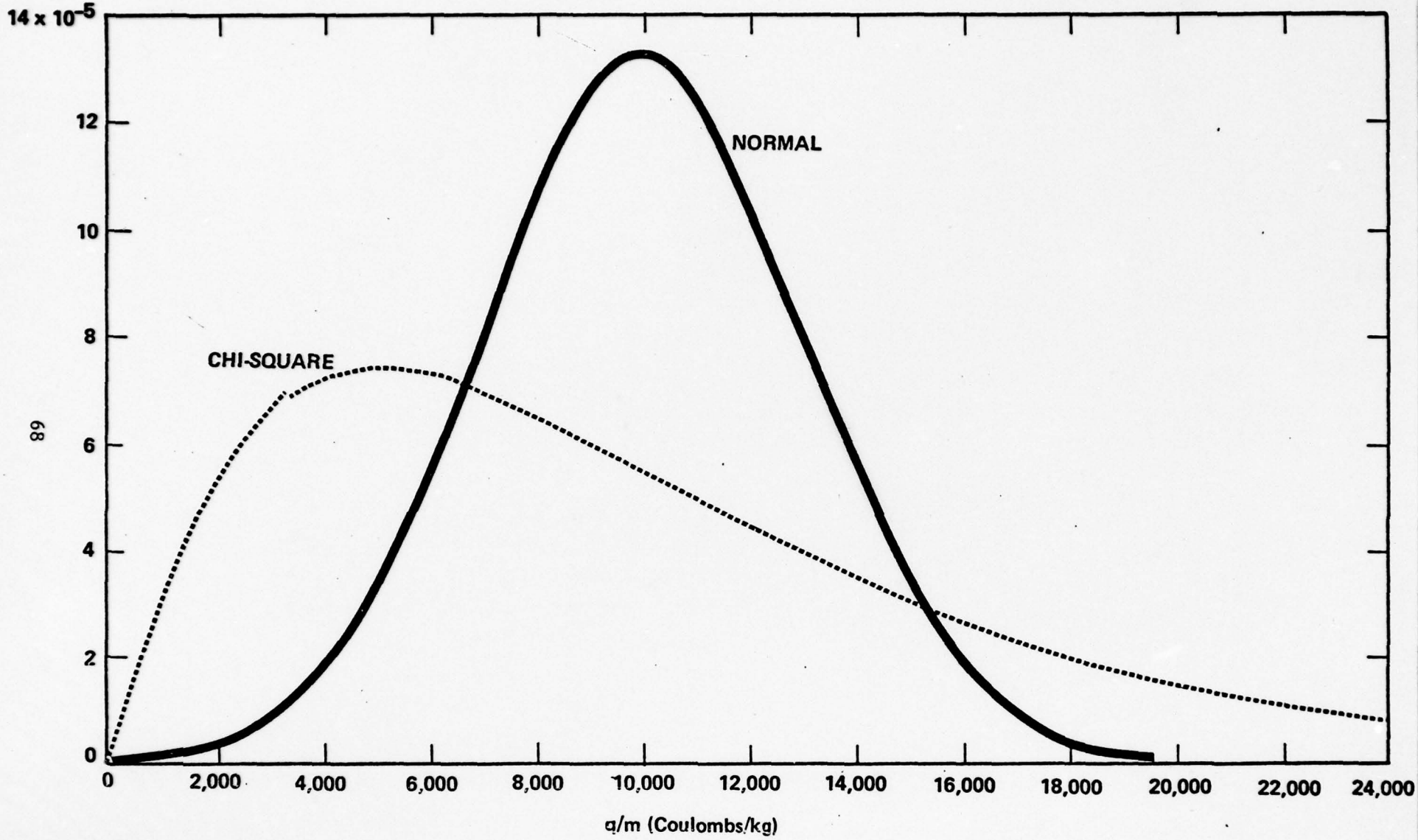

Figure 15. Two Possible Probability Density Functions for q/m

the Chi-Square distribution, therefore, when $\upsilon = 4$, 99 percent of all possible values of z lie in the range

$$0.208 \leq z \leq 14.88 \ .$$

Hence, 99 percent of all possible values of q/m lie in the range

$$520 \leq q/m \leq 37{,}200 \text{ coulombs/kg} \ .$$

Hence,

$$(q/m)_1 = 37{,}200 \text{ coulombs/kg} \ ,$$

$$(q/m)_2 = 520 \text{ coulombs/kg} \ .$$

Except for the limits on the integrals in Eqs. (58) and (62), these two equations remain the same, where, now f(q/m) is given by Eq. (69), and the integral limits are 520 and 37,200. Employing the trapezoidal rule yields:

$$\bar{q} = 9.77 \times 10^{-18} \text{ coulombs},$$

$$\int_{520}^{37{,}200} (q/m)^{-11/6} f(q/m)d(q/m) = 2.537 \times 10^{-7} \text{ (coulombs/kg)}^{-11/6}$$

Hence, Eq. (62) becomes:

$$I(x) = I_o \exp\left[-6.20(10^{-5})\left\{e^{z^2(x)}F[z(x)] - 1.01\ F(z_o)\right\}\right] \qquad (71)$$

Substituting the above in Eq. (41) yields the ion collision rate. The upper solid curve in Figure 14 shows the collision rate versus the axial distance, x, from the tip of the emitter.

5.6 SUMMARY OF DISTRIBUTION RESULTS

The results of the foregoing analysis can be readily summarized in Figure 14 and in Table VI. Essentially five important conclusions can be drawn from the curves in this figure. They are:

a. The most conspicuous characteristics of the four curves in Figure 14 is that the collision rate increases with increasing values of the axial distance, x, reaching a maximum at the termination of the acceleration region.

b. Increasing the standard deviation, S, of the normal distribution also increases the collision rate, for any value of x.

c. The shape of the curves is the same for both the normal ($S \neq 0$) and Chi-Square distributions.

d. The minimum possible lower limit of the integral in Eq. (58), and the first integral in Eq. (62), is $(q/m)_2 = 0$. From Eq. (57), we see that, for $\overline{q/m} = 10{,}000$ coulombs/kg, this minimum lower limit will occur when $S = 3333.33$ coulombs/kg. The value $S = 3300$ coulombs/kg has already been employed in the calculations. From Figure 14, we see that the collision rate for $S = 3300$ coulombs/kg differs, at most, from the collision rate for $S = 0$, by approximately only an order of magnitude.

e. The collision rate corresponding to the Chi-Square distribution, which can be thought of as a skewed normal distribution, is only slightly greater than the collision rate corresponding to the normal distribution, for $S = 3300$ coulombs/kg, at every value of x.

TABLE VI

COLLISION RATES

Probability Density Function f(q/m)	Mean Charge-to mass Ratio (coulombs/kg)	Standard Deviation (coulombs/kg)	Ion Collision Rate (collisions/sec)
Normal (Gaussian)	10,000	0	1.909×10^8
Normal (Gaussian)	10,000	3,000	3.327×10^8
Normal (Gaussian)	10,000	3,300	6.034×10^8
Chi-Square	10,000	7,071	7.907×10^8

SECTION 6

NEGATIVE ION PRODUCTION

6.1 POSSIBLE MECHANISMS FOR NEGATIVE IODINE PRODUCTION

Iodine exists in charged colloid droplets in three forms, NaI, I^-, and I. Negative iodine ions can exist through ionic dissociation of NaI molecules in the glycerol solvent. The presence of atomic iodine atoms in the droplets is probably due to the solubility of iodine in glycerol after iodine ions have lost an electron at the emitter electrode. A collision involving breakup or evaporation of a droplet can release I^- directly by liberating the I^- already present, as indicated in Figure 16. Atomic iodine can also be released and, through a process of low energy attachment, form I^-, since iodine has a high electron affinity. Attachment electrons may be provided from ionization events within the droplet at breakup. Nevertheless, this event has a low probability of occurring, since electron capture only occurs at low energy and the electrons gain high energy very quickly in the intense electric fields.

Negative iodine ions may also be formed in collisions from the dissociation of NaI to form Na^+ and I^-. This reaction, as shown in Figure 16, is less probably than the more energetically favorable dissociation of NaI into its atomic components of Na and I. The latter reaction has a greater probability of occurring but, in high energy collisions of molecular ions with droplets, more than enough energy is available to dissociate NaI into its ionic components.

Evidence that droplets break up in collisions can be inferred from various optical and mass spectra data. The presence of atomic sodium in the colloid thruster beam has been measured by several groups,

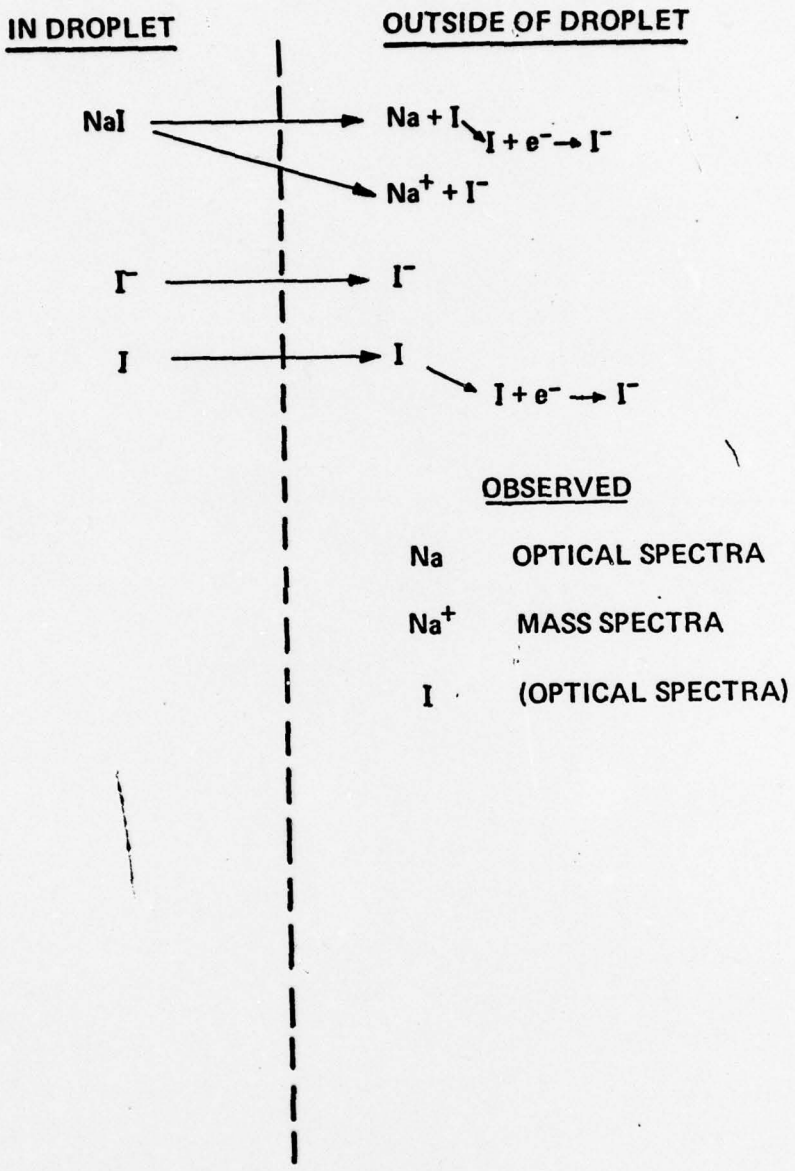

Figure 16. Mechanisms of I^- Production

including TRW, Xerox/EOS, and researchers at the University of Illinois. Some evidence that atomic iodine is present in the colloid exhaust beam was measured by Weinstein.[18] The latter study showed that two and possibly three iodine lines were observed in optical spectra measurements. The identification of atomic sodium and iodine in the colloid beam poses the question concerning their origin. It is presently believed that these atomic species are liberated from droplets which break up in collisions with molecular ions or other droplets. Sodium ions have also been detected using mass spectra technique.

In summary, Na, I, and Na^+ have been observed in the colloid beam. It is plausible to assume that I^- is also present in the exhaust beam. However, I^- has not been measured and this is partly due to the difficulty of observing negative ion species experimentally, and before this study there was little or no interest in even considering searching for I^-.

6.2 NEGATIVE ION TURNAROUND IN ACCELERATION REGION

Atomic or fragment negative ions released during a droplet breakup event will have an initial velocity equal to the velocity of the droplet at the time of breakup. An illustration of the collision and breakup is shown in Figure 17. Whether the negative ion has sufficient energy to escape the electric field in the accelerating region will depend on the charge-to-mass ratio of the negative ion and its velocity at the time of formation.

Consider the one-dimensional case of a charged particle in an electric field. The equation of motion for the particle becomes

$$\frac{d^2x}{dt^2} + C_f \frac{dV(x)}{dx} = 0 , \qquad (63)$$

where $C_f = q/m$ is the fragment or atomic negative ion charge-to-mass ratio. Equation (63) determines the trajectory of the negative particle

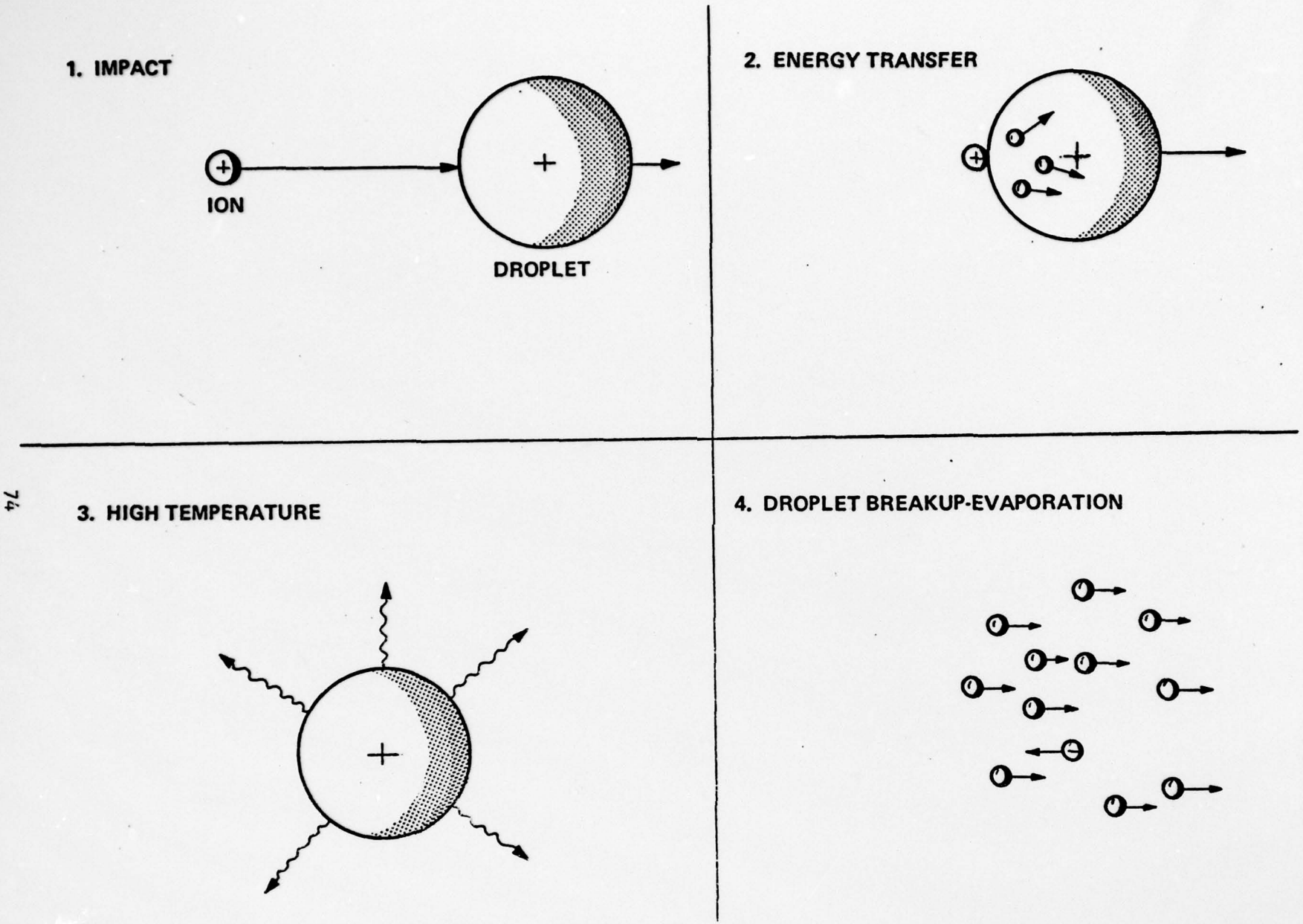

Figure 17. Model of Negative Ion Formation

in the electric field after its formation. It is convenient to solve this equation for the velocity in terms of the potential at droplet breakup, V_B, and the potential at turnaround, V_T, subject to the following boundary conditions:

$$v(x) = v_B;\ V(x) = V_B$$
$$v(x) = 0;\ V(x) = V_T\ . \tag{64}$$

The initial downstream velocity of the negative particle at breakup becomes

$$v_B^2 = 2C_f\ (V_T - V_B)\ . \tag{65}$$

The velocity at breakup, v_B, can also be determined from the original charge-to-mass ratio of the droplet which has been accelerated through a potential difference $\Delta V = V_o - V_B$, where V_o is the potential at the emitter surface. Thus,

$$v_B^2 = 2C_i(V_o - V_B) = 2C_i\,\Delta V\ , \tag{66}$$

where C_i is the charge-to-mass ratio of the droplet before breakup. If we eliminate v_B between Eqs. (67) and (66) and solve for V_T,

$$V_T = V_o - \Delta V\left(1 + \left|\frac{C_i}{C_f}\right|\right). \tag{67}$$

Values for the turnaround potential were computed for the case of the production of negative iodine ions, assuming an initial droplet of 10^4 C/kg and an emitter potential v_o = 13 kV. For this case,

$\left|\frac{C_i}{C_f}\right| = 1.32 \times 10^{-12}$ and values for V_T are shown below at corresponding potentials at breakup:

$V_o = 13$ kV

V_B(kV)	ΔV(kV)	V_T(kV)
12	1	11.98
11	2	10.97
8	5	7.93
5	8	4.89
3	10	2.86
1	12	0.84

These results indicate that negative iodine particles do not continue very far after their formation in the accelerating region. At the boundary of the accelerating region where $V(x) = V_T = 0$, we can solve Eq. (67) for ΔV to obtain

$$\Delta V = \frac{V_o}{\left(1 + \left|\frac{C_i}{C_f}\right|\right)} \tag{68}$$

For iodine negative ions we find $\Delta V = 12.83$ kV. Therefore, iodine ions formed after a droplet has been accelerated through a potential difference greater than 12.83 kV will escape the accelerating region ($V_o = 13$ kV). We conclude from this analysis that nearly all the negative iodine ions formed within the accelerating region do notescape and will be accelerated toward the emitter.

SECTION 7

CONCLUSIONS AND RECOMMENDATIONS

7.1 SUMMARY OF THE MODEL

This report has presented the essential features of a model describing the mechanisms of colloid emitter damage responsible for the degradation of performance. The model is summarized here and the reference section listed.

		Section
a.	Particle species in the exhause charged droplets	(3)
	Charged droplets	
	Molecular ions	
	Neutral molecules	
	Electrons	
b.	Highest density of particles in the portion of the exhaust beam within the acceleration region	(3)
	Molecular ion current density $\approx 6 \times 10^{12}$ ions/sec	(3.2)
	Charged droplet density $\approx 10^{9}/cm^{3}$	(3.3)
	Neutral molecules $\approx 10^{9}$ molecules/cm^{3}	(3.1)
	Electrons, very few expected.	
c.	Charged droplet distribution is represented by the mean charge-to-mass ratio.	(3.4)
d.	The mean droplet has a total molecular binding energy of $\approx$ 3 keV.	(3.4)
e.	The acceleration region also has a highly divergent and intense electric field.	(2.2)
f.	Collisions will occur between these particle species because they travel with greatly different velocities.	(4)

		Section
g.	Only collisions between charged droplets and both molecular ions and electrons could cause droplet breakup.	(4)
h.	Molecular ion collisions with charged droplets occur at the highest rate because of the current densities and collision cross sections. These rates range between 10^8 and 10^9/sec. Inclusion of small droplet collisions with large droplets increases the above rate.	(4.3)
i.	Droplet fragment particles have been observed experimentally, providing evidence of collisions.	(4.1)
j.	Charged droplets may decrease in size due to evaporation and result in positive charge emission. This is not likely to lead to negative ion production.	(4.4)
k.	Several distributions of particle sizes were introduced into the model and compared with the single particle model.	(5)
l.	Normal distributions having various standard deviations and also a Chi-square distribution were used with no significant alteration of the results.	(5)
m.	When molecular ions collide with droplets, the droplets break up due to the deposition of the ion energy in the droplet.	(4.3)
n.	Several processes are advanced for the production of negative iodine at the collisional breakup of a droplet.	(6.1)
o.	All negative ions (I^-) produced in the acceleration region from the breakup of droplets, except for a few near the edge of the acceleration region, do not escape from the region.	(6.2)
p.	These negative ions are returned to the emitter and bombard the surface with energies of several thousand electron volts.	(6.2)
q.	Each ion sputters between 1 and 10 atoms from the emitter surface, depending upon the bombarding ion energy.	(2.3)
r.	The observed erosion is adequately explained by this model if, on the average, each molecular ion/droplet collision results in the production of one negative ion.	(2.3)

	Section
s. The eroded emitter surface causes a change in the intense electric field at the emitter.	(2.1)
t. Alteration of the field at the emitter results in degradation of performance.	(2.1)

7.2 SUGGESTED EXPERIMENTS FOR DETECTION OF NEGATIVE IONS

Investigations into the possible mechanisms of negative ion production suggest several experimental directions. Understanding of the colloid emitter erosion process may require a two-phase experimental approach. One experimental phase would treat the problem of detecting negative ions and identifying the species. Measurements using mass spectrometer techniques will yield this type of information. Other experiments could be designed to provide information concerning the mechanism of negative ion formation.

Two experimental directions have been considered to provide data that could verify models of negative ion formation. One such experiment would involve a cross-beam technique using two colloid sources. One source would be operated in the molecular ion emission mode and one operated in the heavy charged droplet mode. If I^- or other negative ions are released during droplet breakup collisions, absorption spectra may provide a suitable detection method. A less direct approach for testing the hypothesis of negative iodine liberation in droplet collisions involves absorption spectra measurements in the region of a collector downstream from a colloid source. Droplet impact at the collector involves higher collision energies than are generally available within the accelerating region, but, nevertheless, may provide useful clues as to the formation and type of negative ions produced when charged droplets break up. In both droplet breakup experiments suggested above, mass spectrometer measurements could be substituted for absorption spectroscopy to detect negative ions.

7.3 RECOMMENDATIONS

To reduce emitter erosion and the subsequent performance degradation, several recommendations were made:

a. Operation at lower voltages would reduce the bombardment energies of the negative ions and, therefore, the sputtering rate.

b. Use a propellant dopant having a much lower mass than iodine to reduce the sputtering rate.

c. Use an emitter material having a lower sputtering yield.

d. Use a propellant containing no atoms or molecules having a significant electron affinity, thus reducing the production of negative ions.

e. Eliminate the productivity of positive ions at the emitter which therefore reduces the ion/droplet collision rate. Elimination of positive ion production also increases the efficiency of the thruster operation.

REFERENCES

1. J. F. Mahoney and J. Perel, "Particle Interactions in Colloid Exhaust Plumes," Paper 76-1056, AIAA 12th Electric Propulsion Conference, Key Biscayne, Florida (15 Nov 1976).

2. S. Zafran, "Colloid Advanced Development Program," Contract Status Report, TRW Systems, Redondo Beach, CA, Report No. 48 (15 Jun 1974); Report No. 51, (15 Sep 1974).

3. H. D. Beckey, H. Krone, and F. W. Roellgen, "Comparison of Tips, Thin Wires and Sharp Metal Edges for Field Ionization Mass Spectrometry," J of Sci. Inst., V. 1, p. 118, 1968.

4. M. N. Huberman, P. W. Kidd, "Charged Particle Electrostatic Thrusters," Tech. Report AFAPL-TR-69-14, p. 57, Mar 1969.

5. J. E. Cox and P. W. Kidd, "Effects of Long Term Operation on Advanced Colloid Engine Performance," AIAA 11th Elec. Prop. Conf., Paper No. 75-393 (New Orleans, LA, Mar 19-21, 1975).

6. K. Kanaya, K. Hojou, K. Koga, and K. Toki, "Consistency Theory of Sputtering of Solid Targets by Ion Bombardment Using Power Potential Law," Jap. J ofAppl. Phys., V. 12, p. 1297, Sep 1973.

7. J. B. Hasted, Physics of Atomic Collisions, p. 67, Butterworths Publisher (Washington, 1964).

8. S. Dushman, Scientific Foundations of Vacuum Technique, 2nd Edition, John Wiley & Sons, Inc., p. 18.

9. F. R. McFeely and G. A. Somorjai, "Studies of the Vaporization Kinetics of Hydrogen-Bonded Liquids," J. Phy. Chem., V. 76, p. 914, 1972.

10. D. S. Simons, B. N. Colby, and C. A. Evans, Jr., "Electrohydrodynamic Ionization Mass Spectrometry - The Ionization of Liquid Glycerol and Non-Volatile Organic Solutes," Int. J. of Mass Spec. and Ion Physics, V. 15, p. 291 (1974).

11. M. A. Rizk and I. M. Elanwar, "Dipole Moments of Glycerol, Isopropyl Alcohol, and Isobutyl Alcohol," Can. J. of Chem., V. 46, p. 507, 1968.

12. Y. K. Syrkin and M. E. Dyatkina, Structure of Molecules and the Chemical Bond, p. 197, Dover Publications, Inc., New York, 1964.

13. I. Langmuir, Phenomena, Atoms and Molecules, p. 224, Philosophical Library, New York (1950).

14. Y. K. Dyrkin and M. E. Dyatkina, Structure of Molecules and the Chemical Bond, p. 197, Dover Publications, Inc., New York, 1964.

15. G. Burrow, "Some Consequences of the Behavior of Mobile Molecules," Vacuu, V. 2 and 3, p. 3 (1957-8).

16. H. B. Gray, Chemical Bonds: An Introduction to Atomic and Molecular Structure, p. 199, W. A. Benjamin, Inc., 1973.

17. Fred W. McLafferty, "Mass Spectrometric Analysis," Anal. Chemistry, V. 28, p. 306 (1956).

18. B. Weinstein, "High Current Ion Emission in LID Spraying," Thesis, University of Illinois, Urbana, Ill., Jun 1975 (Unpublished).

19. Marton, L., ed., Advances in Electronics and Electron Physics, Vol. XIII, p. 100 (1956).

20. "Radiation Research Reviews," 3, p. 69 (1971).

21. L. Katz and A. S. Penfold, Revs. Mod. Phys., 24, 28 (1952).

22. R. D. Evans, The Atomic Nucleus, p. 583, McGraw-Hill (1955).

23. P. Dalton and J. E. Turner, "New Evaluation of Mean Excitation Energies for Use in Radiation Dosimetry," Health Physics, V. 15, p. 257 (1968).

24. E. Jahnke and F. Emde, Tables of Functions, p. 32, Dover Publications (1945).

25. M. A. Abbas and J. Latham, J. Fluid Mech., 30, 663 (1967).

26. N. K. Adam, The Physics & Chemistry of Surfaces, Dover Publications, New York, 1968, p. 14.